Virtual Institute of Astroparticle Physics (VIA)

Lecture,　29 Nov. 2013

Gravitational lensing by exotic objects

Hideki Asada

(Hirosaki U)

You may immediately say,
“it is not surprising that a lot of changes are caused by exotic lenses.”

Please enjoy what changes appear.

Why did Hirosaki group start it?

Frankly speaking, I had never worked on this exotic subject but one day ...

One of my undergrad students (Toki-kun) was so interested in Abe-san seminar talk on wormholes in Hirosaki (Dec. 2010).

Graduation thesis (“sotsu-ron”) calculations were done by Toki-kun and Kitamura-kun. (Jan-Mar. 2011)

The Astrophysical Journal, 740:121 (8pp), 2011 October 20 doi:10.1088/0004-637X/740/2/121

ASTROMETRIC IMAGE CENTROID DISPLACEMENTS DUE TO GRAVITATIONAL MICROLENSING BY THE ELLIS WORMHOLE

Yukiharu Toki[1], Takao Kitamura[1], Hideki Asada[1], and Fumio Abe[2,3]
[1] Faculty of Science and Technology, Hirosaki University, Hirosaki 036-8561, Japan
[2] Solar-Terrestrial Environment Laboratory, Nagoya University Furo-cho, Chikusa-ku, Nagoya 464-8601, Japan; abe@stelab.nagoya-u.ac.jp
Received 2011 April 26; accepted 2011 July 22; published 2011 October 4

ABSTRACT

Continuing work initiated in an earlier publication, we study the gravitational microlensing effects of the Ellis wormhole in the weak-field limit. First, we find a suitable coordinate transformation, such that the lens equation and analytic expressions of the lensed image positions can become much simpler. Second, we prove that two images always appear for the weak-field lens by the Ellis wormhole. By using these analytic results, we discuss astrometric image centroid displacements due to gravitational microlensing by the Ellis wormhole. The astrometric image centroid trajectory by the Ellis wormhole is different from the standard one by a spherical lensing object that is expressed by the Schwarzschild metric. The anomalous shift of the image centroid by the Ellis wormhole lens is smaller than that by the Schwarzschild lens, provided that the impact parameter and the Einstein ring radius are the same. Therefore, the lensed image centroid by the Ellis wormhole moves slower. Such a difference, although it is very small, will be, in principle, applicable for detecting or constraining the Ellis wormhole by using future high-precision astrometry observations. In particular, the image centroid position gives us additional information, so that the parameter degeneracy existing in photometric microlensing can be partially broken. The anomalous shift reaches the order of a few micro arcseconds, if our galaxy hosts a wormhole with throat radius larger than 10^5 km. When the source moves tangentially to the Einstein ring, for instance, the maximum position shift of the image centroid by the Ellis wormhole is 0.18 normalized by the Einstein ring radius. For the same source trajectory, the maximum difference between the centroid displacement by the Ellis wormhole lens and that by the Schwarzschild one with the same Einstein ring radius is -0.16 in the units of the Einstein radius, where the negative means that the astrometric displacement by the Ellis wormhole lens is smaller than that by the Schwarzschild one.

Wormholes (WHs) attract many theorists, especially since Morris and Thorne (1988)

Light propagation in Ellis worm-hole gravity, especially deflection angle of light, is repeatedly discussed.

[8] L. Chetouani and G. Clément, Gen. Relativ. Gravit. **16**, 111 (1984).

[9] G. Clément, Int. J. Theor. Phys. **23**, 335 (1984).

[10] V. Perlick, Phys. Rev. D **69**, 064017 (2004).

[11] M. Safonova, D. F. Torres, and G. E. Romero, Phys. Rev. D **65**, 023001 (2001).

[12] A. A. Shatskii, Astronomy Reports **48**, 525 (2004).

[13] K. K. Nandi, Y. Z. Zhang, and A. V. Zakharov, Phys. Rev. D **74**, 024020 (2006).

[14] F. Abe, Astrophys. J. **725**, 787 (2010).

[16] T. K. Dey and S. Sen, Mod. Phys. Lett. A **23**, 953 (2008).

[17] A. Bhattacharya and A. A. Potapov, Mod. Phys. Lett. A **25**, 2399 (2010).

[19] K. Nakajima and H. Asada, Phys. Rev. D **85**, 107501 (2012).

[20] G. W. Gibbons and M. Vyska, Classical Quantum Gravity **29**, 065016 (2012).

PHYSICAL REVIEW D **69**, 064017 (2004)

Exact gravitational lens equation in spherically symmetric and static spacetimes

Volker Perlick*
Institut für Theoretische Physik, Universität zu Köln, Zülpicher Str. 77, 50937 Köln, Germany
(Received 15 July 2003; published 17 March 2004)

Lensing in a spherically symmetric and static spacetime is considered, based on the lightlike geodesic equation without approximations. After fixing two radius values r_O and r_S, lensing for an observation event somewhere at r_O and static light sources distributed at r_S is coded in a lens equation that is explicitly given in terms of integrals over the metric coefficients. The lens equation relates two angle variables and can be easily plotted if the metric coefficients have been specified; this allows us to visualize in a convenient way all relevant lensing properties, giving image positions, apparent brightnesses, image distortions, etc. Two examples are treated: lensing by a Barriola-Vilenkin monopole and lensing by an Ellis wormhole.

IOP PUBLISHING CLASSICAL AND QUANTUM GRAVITY

Class. Quantum Grav. **29** (2012) 065016 (19pp) doi:10.1088/0264-9381/29/6/065016

The application of Weierstrass elliptic functions to Schwarzschild null geodesics

G W Gibbons[1,2] **and M Vyska**[2]

$$\frac{\delta\phi}{\pi} = -\frac{1}{4}\mu^2 - \frac{1}{2}\mu^3 - \frac{41}{64}\mu^4 - \frac{9}{16}\mu^5 - \frac{25}{256}\mu^6 + \frac{37}{128}\mu^7 + \frac{11\,959}{16\,384}\mu^8 + \frac{1591}{2048}\mu^9 + \frac{13\,311}{65\,536}\mu^{10} - \frac{29\,477}{32\,768}\mu^{11} - \cdots. \tag{139}$$

PHYSICAL REVIEW D **85,** 107501 (2012)

Deflection angle of light in an Ellis wormhole geometry

Koki Nakajima and Hideki Asada

Faculty of Science and Technology, Hirosaki University, Hirosaki 036-8561, Japan

(Received 1 March 2012; published 3 May 2012)

Dey and Sen (2008) formula

$$\alpha = \pi\left\{\sqrt{\frac{2(r_0^2 + a^2)}{2r_0^2 + a^2}} - 1\right\},$$

The correct one is derived as

(Perlick, Gibbons and Vyska, Nakajima and HA)

$$\alpha(b) = 2\int_0^1 \frac{dt}{\sqrt{(1-t^2)(1-k^2t^2)}} - \pi = 2K(k) - \pi, \tag{9}$$

where $t \equiv b/R$ and $k \equiv a/b$. The integral in Eq. (9) is a complete elliptic integral of the first kind $K(k)$, which admits a series expansion for $k < 1$. Hence, Eq. (9) is expanded as

$$\alpha(b) = \pi\sum_{n=1}^{\infty}\left[\frac{(2n-1)!!}{(2n)!!}\right]^2 k^{2n}. \tag{10}$$

Raychaudhuri's equation for null geodesics

$$\dot{\hat{\theta}} = -\frac{1}{2}\hat{\theta}^2 - 2\hat{\sigma}^2 + 2\hat{\omega}^2 - T_{\mu\nu}U^\mu U^\nu$$

$$T\mu\nu U^\mu U^\nu \geq 0$$

Null Energy Condition

But, exotic objects (e.g. wormholes) may violate Null Energy Condition.

Ricci focusing may be negative, while Weyl focusing is positive.

[N.B., Wormholes without exotic matter in Einstein-Gauss-Bonnet-Dilaton gravity, Kanti+, PRL (2011)]

The Astrophysical Journal, 725:787–793, 2010 December 10 doi:10.1088/0004-637X/725/1/787

GRAVITATIONAL MICROLENSING BY THE ELLIS WORMHOLE

F. Abe
Solar-Terrestrial Environment Laboratory, Nagoya University, Furo-cho, Chikusa-ku, Nagoya 464-8601, Japan; abe@stelab.nagoya-u.ac.jp
Received 2010 February 21; accepted 2010 October 7; published 2010 November 19

ABSTRACT

A method to calculate light curves of the gravitational microlensing of the Ellis wormhole is derived in the weak-field limit. In this limit, lensing by the wormhole produces one image outside the Einstein ring and another image inside. The weak-field hypothesis is a good approximation in Galactic lensing if the throat radius is less than 10^{11} km. The light curves calculated have gutters of approximately 4% immediately outside the Einstein ring crossing times. The magnification of the Ellis wormhole lensing is generally less than that of Schwarzschild lensing. The optical depths and event rates are calculated for the Galactic bulge and Large Magellanic Cloud fields according to bound and unbound hypotheses. If the wormholes have throat radii between 100 and 10^7 km, are bound to the galaxy, and have a number density that is approximately that of ordinary stars, detection can be achieved by reanalyzing past data. If the wormholes are unbound, detection using past data is impossible.

Model

Ellis WH(1973)

$$ds^2 = dt^2 - dr^2 - (r^2 + a^2)(d\theta^2 + \sin^2(\theta) d\phi^2), \qquad (1)$$

Deflection angle of light in weak field approx.

$$\alpha(r) \to \frac{\pi}{4}\frac{a^2}{r^2} - \frac{5\pi}{32}\frac{a^4}{r^4} + o\left(\frac{a}{r}\right)^6 . \qquad (3)$$

(r^{-1} for Sch)

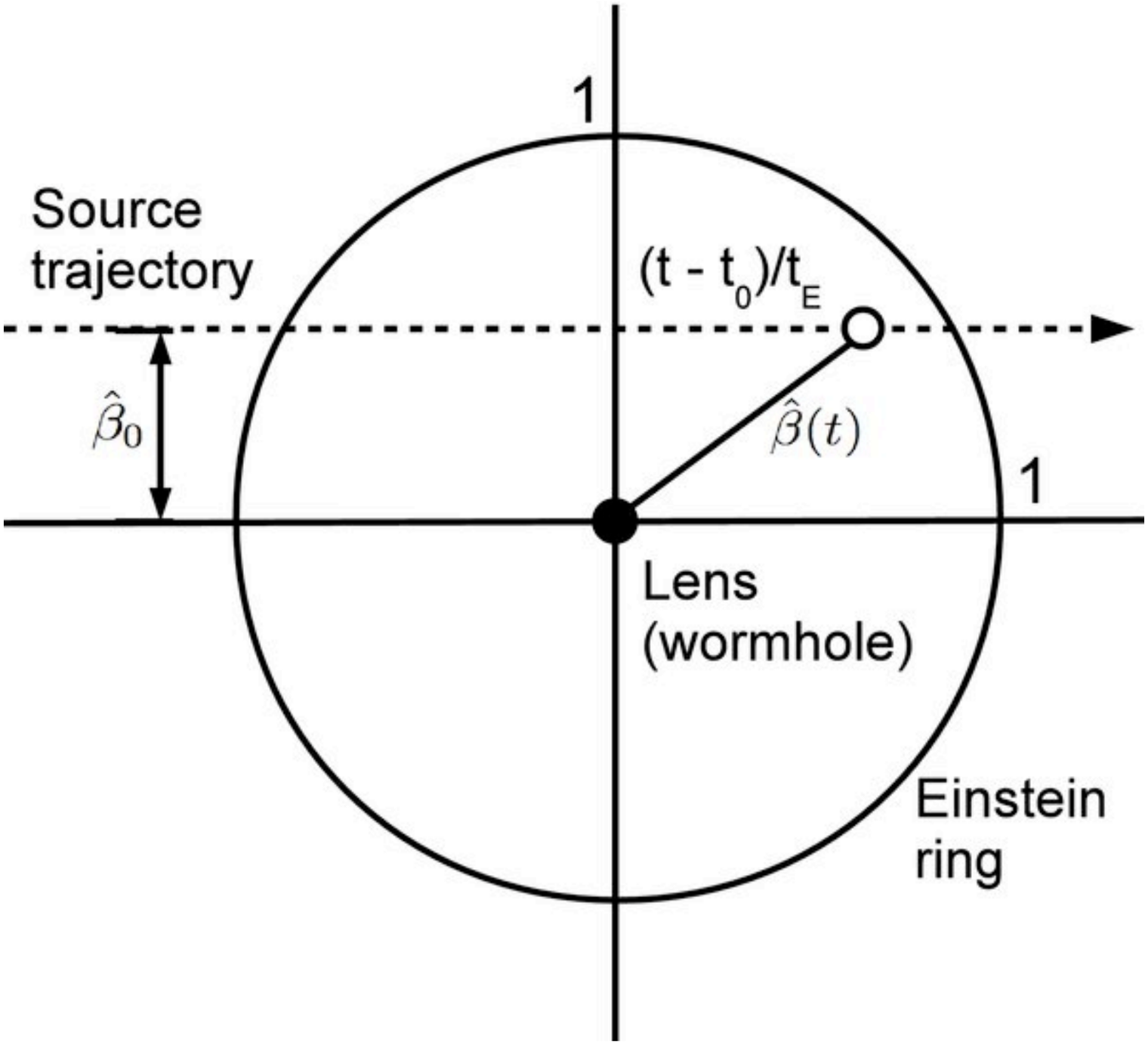
1
Source
trajectory
(t - t0)/tE
β̂0
β̂(t)
1
Lens
(wormhole)
Einstein
ring

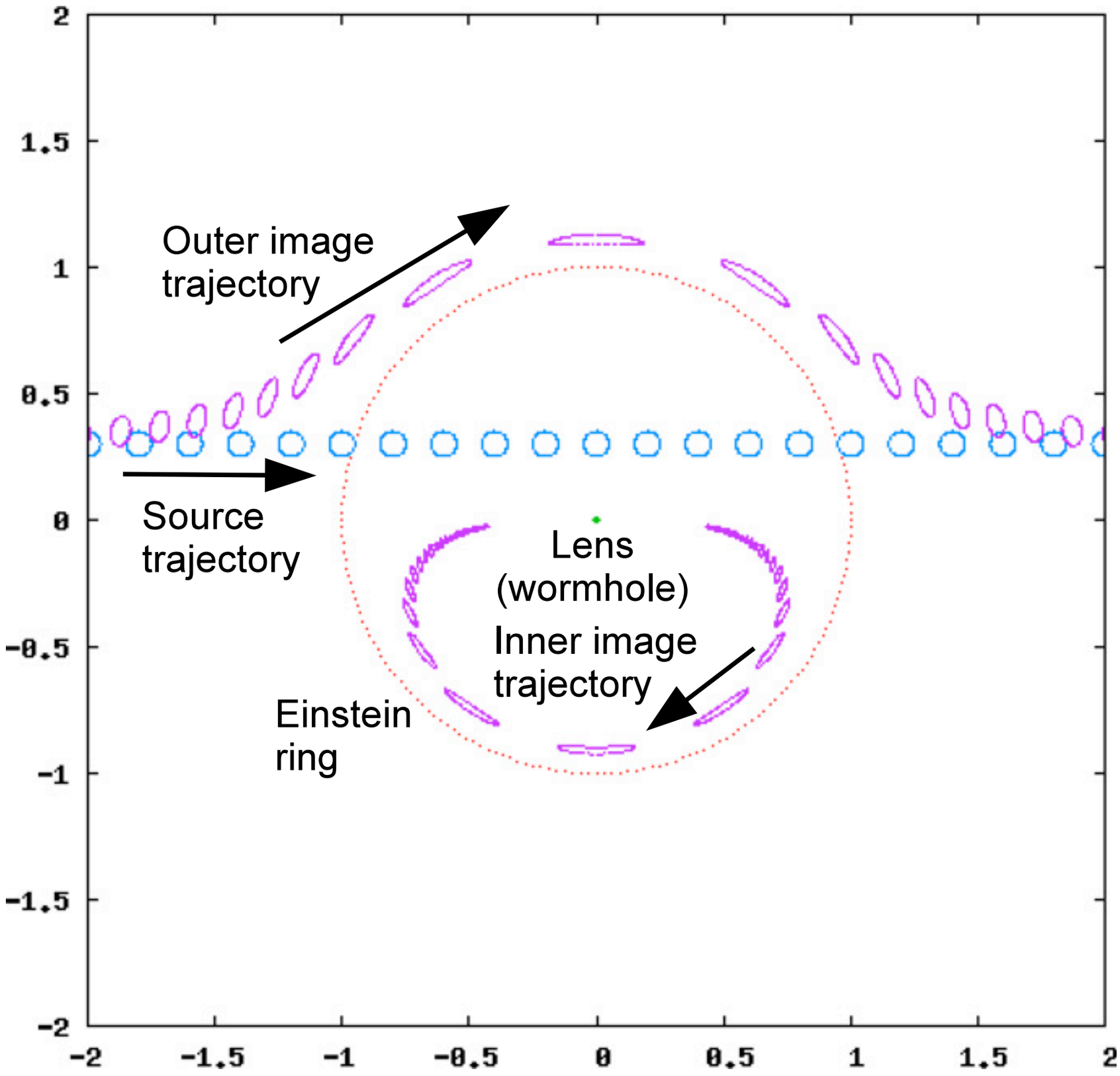
Outer image
trajectory
Source
trajectory
Lens
(wormhole)
Inner image
trajectory
Einstein
ring
2
1.5
1
0.5
0
-0.5
-1
-1.5
-2
-2
-1.5
-1
-0.5
0
0.5
1
1.5
2

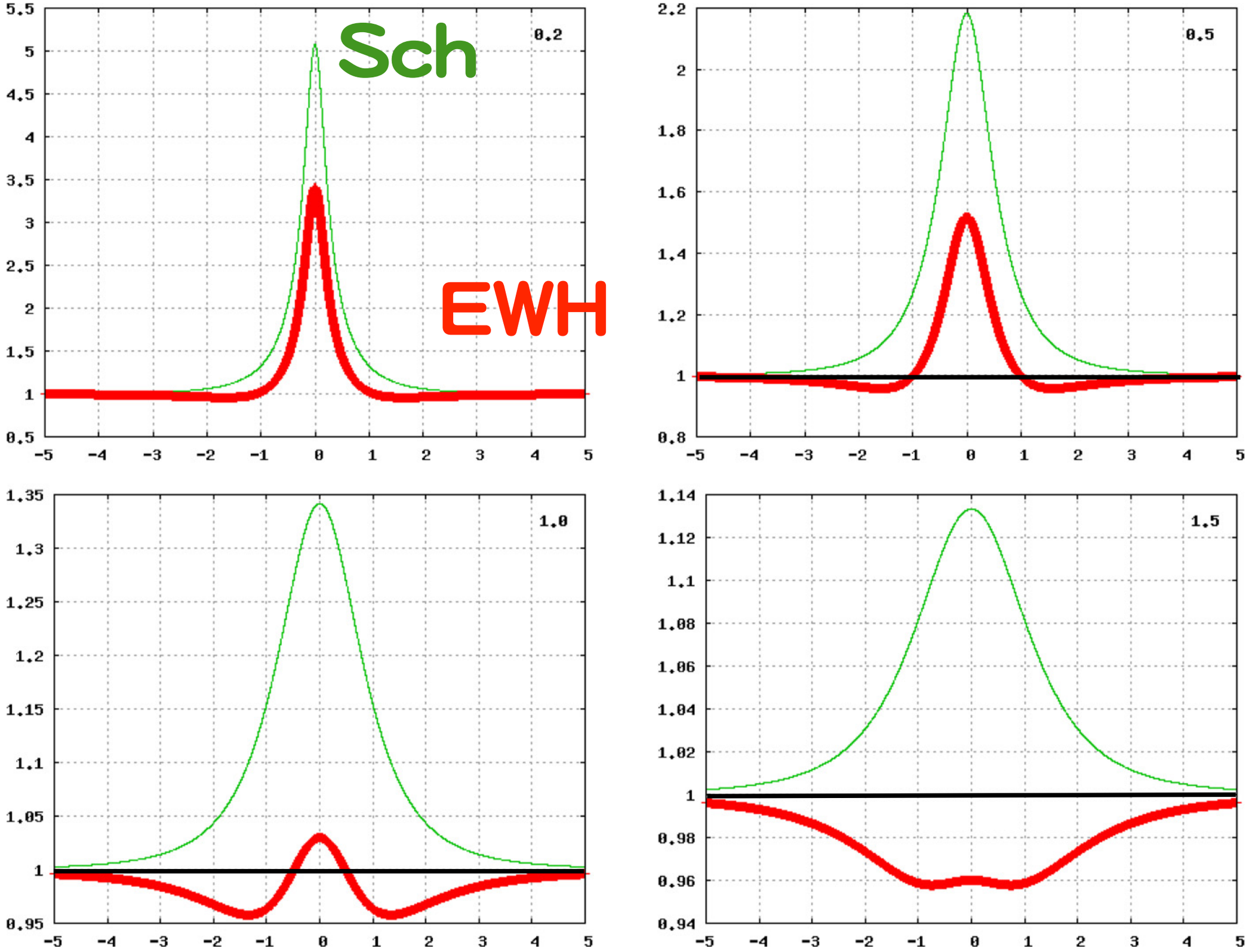

Figure 4. Light curves for $\hat{\beta}_0 = 0.2$ (top left), $\hat{\beta}_0 = 0.5$ (top right), $\hat{\beta}_0 = 1.0$ (bottom left), and $\hat{\beta}_0 = 1.5$ (bottom right). Thick red lines are the light curves for wormholes. Thin green lines are corresponding light curves for Schwarzschild lenses.

(A color version of this figure is available in the online journal.)

1st quiz:

Does demagnification prove wormholes?

To answer this,
let us introduce a one-parameter
model of a weak-field metric

$$ds^2 = -\left(1 - \frac{\varepsilon_1}{r^n}\right)dt^2 + \left(1 + \frac{\varepsilon_2}{r^n}\right)dr^2$$
$$+ r^2(d\theta^2 + \sin^2\theta d\phi^2) + O(\varepsilon_1^2, \varepsilon_2^2, \varepsilon_1\varepsilon_2),$$

(1) static and asymptotically flat

(2) only in the weak field

(3) n=1 ==> Schwarzschild (Sch)
n=2 ==> Ellis Worm Hole (EWH)

(4) n>1 ==> zero ADM mass

After a conformal transformation,

$$d\bar{s}^2 = -dt^2 + \left(1 + \frac{\varepsilon}{R^n}\right) dR^2 + R^2(d\theta^2 + \sin^2\theta d\phi^2)$$
$$+ O(\varepsilon^2),$$

where $\varepsilon \equiv n\varepsilon_1 + \varepsilon_2$ and

$$R^2 \equiv \frac{r^2}{(1 - \frac{\varepsilon_1}{r^n})}.$$

Deflection angle of light is calculated in the textbook manner as

$$\alpha = 2\int_{R_0}^{\infty} \frac{d\phi(R)}{dR}\, dR - \pi = \frac{\varepsilon}{b^n} \int_0^{\frac{\pi}{2}} \cos^n \psi \, d\psi + O(\varepsilon^2),$$

$$\int_0^{\frac{\pi}{2}} \cos^n \psi \, d\psi = \frac{(n-1)!!}{n!!} \frac{\pi}{2} (\text{even } n),$$

$$= \frac{(n-1)!!}{n!!} (\text{odd } n),$$

$$= \frac{\sqrt{\pi}}{2} \frac{\Gamma(\frac{n+1}{2})}{\Gamma(\frac{n+2}{2})} (\text{real } n > 0).$$

always positive constant

Deflection angle of light is simply written as

$$\alpha(b) = \bar{\varepsilon}/b^n$$

n=0 ==> Singular Isothermal Sphere (SIS)

n=1 ==> Sch.

n=2 ==> Ellis Worm Hole (EWH)

This one-parameter model is used also by Tsukamoto and Harada (2012, 2013).

2nd quiz:

How exotic is this lens model?

In the standard lens theory (in GR), convergence (surface mass density) is

$$\kappa(b) = \frac{\bar{\varepsilon}(1-n)}{2} \frac{1}{b^{n+1}}$$

If $\varepsilon > 0$ and $n > 1$, negative convergence

(==> divergent)

Analogies to opical lenses ---

convex lens

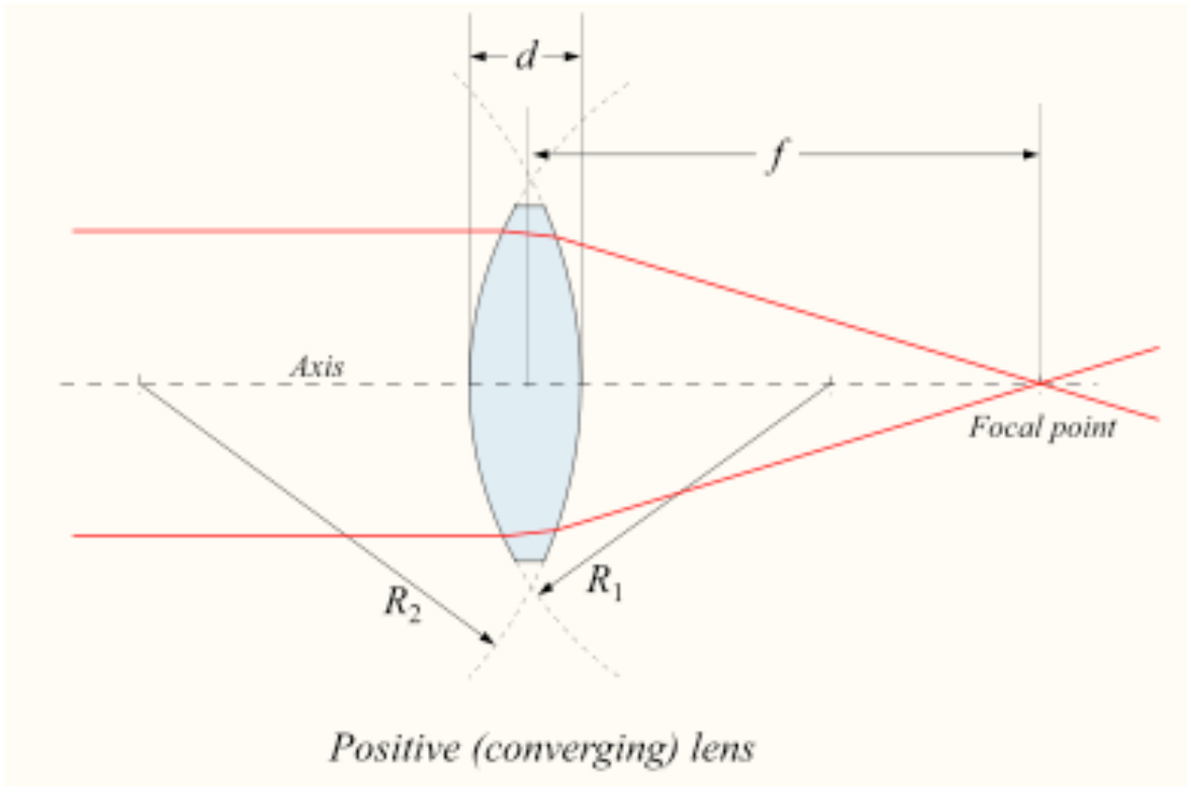

concave lens

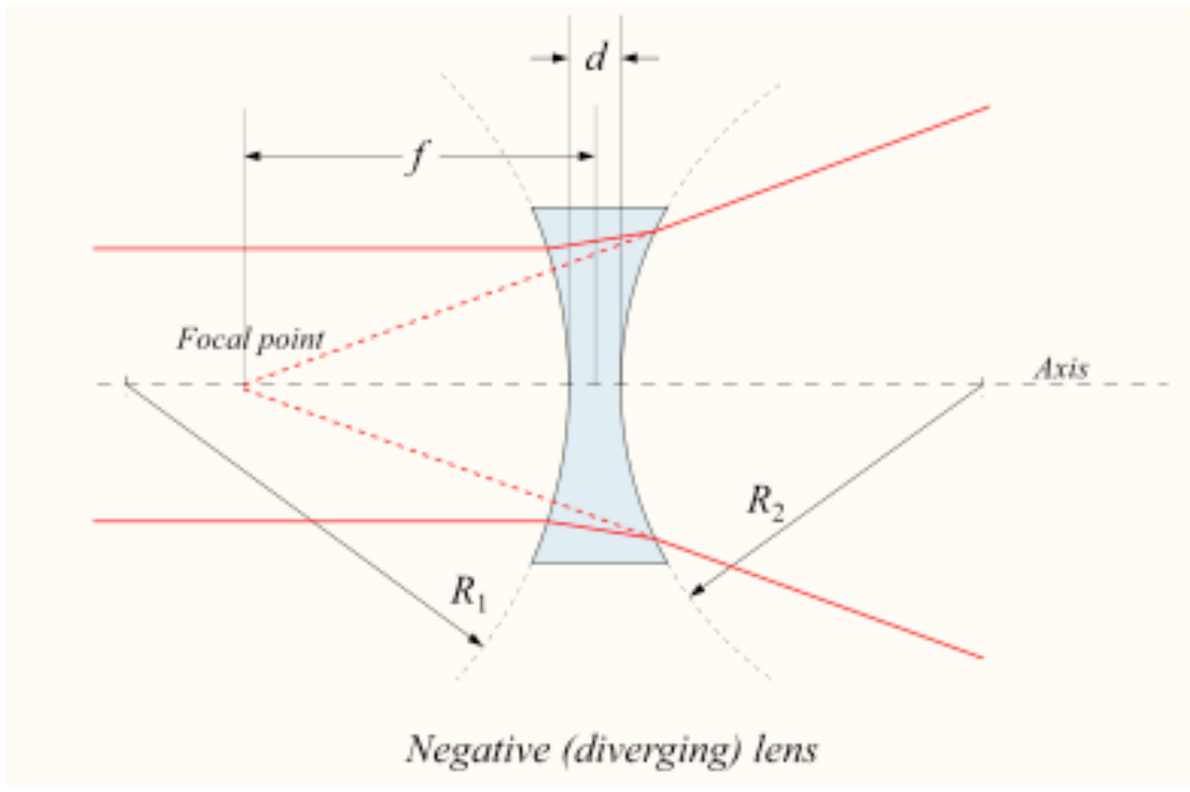

$\kappa > 0$

$\kappa < 0$

“Standard” Grav Lens

“Diversing”

can express both positive and negative

$\kappa > 0$ Non-vac. Ricci-focusing	$\varepsilon > 0$ & $n < 1$	SIS
	$\varepsilon < 0$ & $n > 1$	
Vac. $\kappa = 0$ Weyl-focusing	$n = 1$	Sch
$\kappa < 0$ Non-vac. Ricci-defocusing	$\varepsilon > 0$ & $n > 1$	EWH
	$\varepsilon < 0$ & $n < 1$	

Lens Equation with thin lens approx.

$$\beta = \frac{b}{D_L} - \frac{D_{LS}}{D_S}\alpha(b)$$

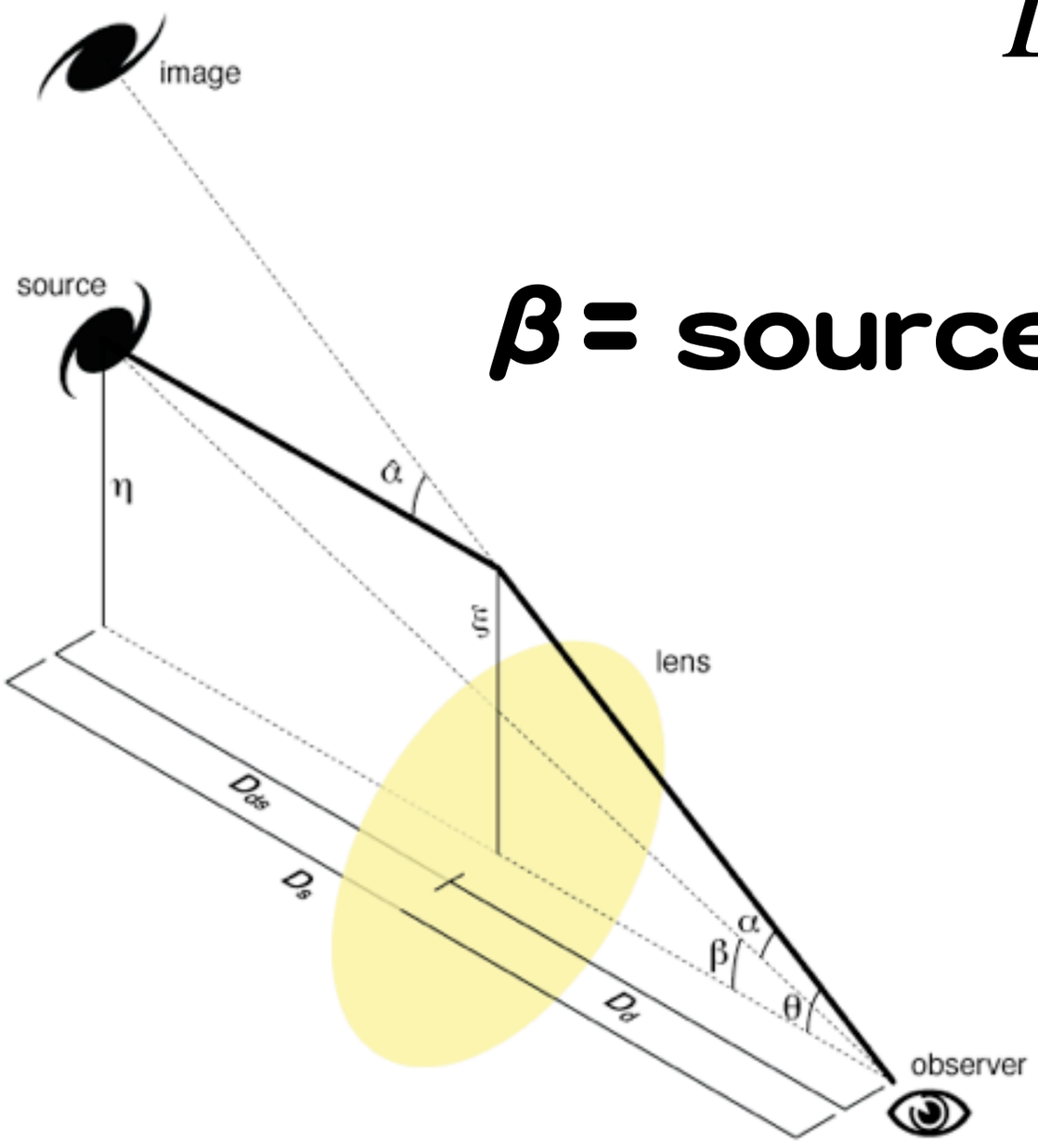

β = source angular position

For $\varepsilon > 0$,

Einstein ring for $\beta = 0$

$$\theta_{\mathrm{E}} \equiv \left(\frac{\bar{\varepsilon} D_{LS}}{D_S D_L^n} \right)^{\frac{1}{n+1}}.$$

If $\varepsilon < 0$,

(tentative) Einstein ring radius

$$\theta_{\mathrm{E}} \equiv \left(\frac{|\bar{\varepsilon}| D_{LS}}{D_S D_L^n} \right)^{\frac{1}{n+1}},$$

$$\text{If } \varepsilon < 0,$$

repulsive
like a concave lens

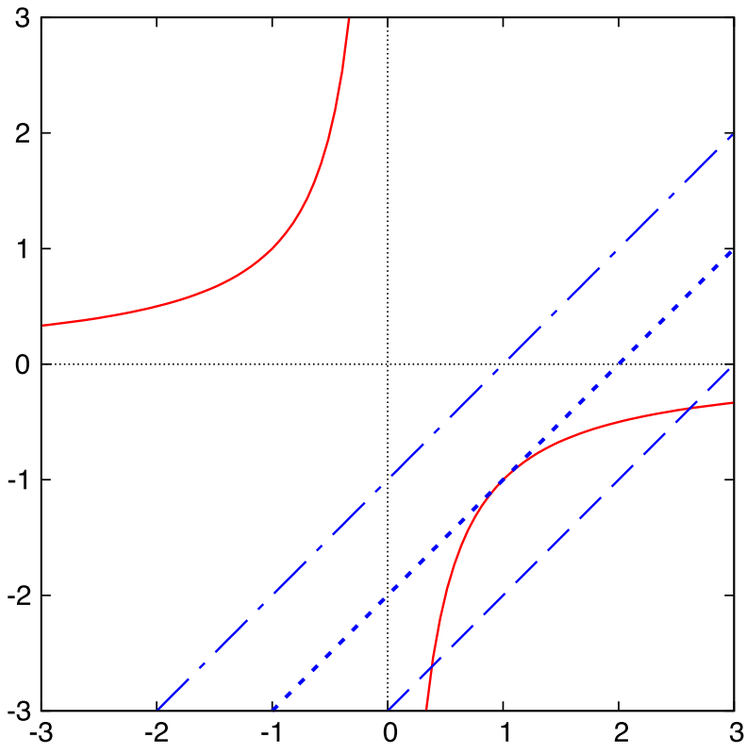

0 images

1 images

2 images

FIG. 3 (color online). Repulsive lens model ($\varepsilon < 0$). Solid curves denote $1/\hat{\theta}^n$ and straight lines mean $\hat{\theta} - \hat{\beta}$. Their intersections correspond to image positions that are roots for the lens equation. There are three cases: No image for a small $\hat{\beta}$ (dot-dashed line), a single image for a particular $\hat{\beta}$ (dotted line), and two images for a large $\hat{\beta}$ (dashed line). The two images are on the same side of the lens object.

Let us study three astronomical observables as

1) Image brightness (micro-lens)

2) Image shape (macro-lens)

3) Image motion (micro-lens)

Image brightness(micro)

PHYSICAL REVIEW D **87,** 027501 (2013)

Demagnifying gravitational lenses toward hunting a clue of exotic matter and energy

Takao Kitamura, Koki Nakajima, and Hideki Asada

Faculty of Science and Technology, Hirosaki University, Hirosaki 036-8561, Japan

(Received 3 November 2012; published 10 January 2013)

$$\hat{\beta} \equiv \beta/\theta_E \text{ and } \hat{\theta} \equiv \theta/\theta_E$$

$$\hat{\beta} = \hat{\theta} - \frac{1}{\hat{\theta}^n} \quad (\hat{\theta} > 0),$$

$$\hat{\beta} = \hat{\theta} + \frac{1}{(-\hat{\theta})^n} \quad (\hat{\theta} < 0),$$

For small beta (source is close to lens)

$$\hat{\theta}_+ = 1 + \frac{1}{n+1}\hat{\beta} + \frac{1}{2}\frac{n}{(n+1)^2}\hat{\beta}^2 + O(\hat{\beta}^3) \quad (\hat{\theta} > 0), \tag{9}$$

$$\hat{\theta}_- = -1 + \frac{1}{n+1}\hat{\beta} - \frac{1}{2}\frac{n}{(n+1)^2}\hat{\beta}^2 + O(\hat{\beta}^3) \quad (\hat{\theta} < 0). \tag{10}$$

Axisymmetric along l.o.s.

$$A \quad \text{is} \quad |(\beta/\theta) \times (d\beta/d\theta)|^{-1},$$

$$A_\pm = \frac{1}{\hat{\beta}(n+1)} + O(\hat{\beta}^0),$$

$$A_{\rm tot} \equiv A_+ + A_- = \frac{2}{\hat{\beta}(n+1)} + O(\hat{\beta}^0). \qquad (12)$$

Total demagnification (A_tot < 1) occurs, iff

$$\hat{\beta} > \frac{2}{n+1}$$

under weak field + thin lens + small beta approximations

Sch

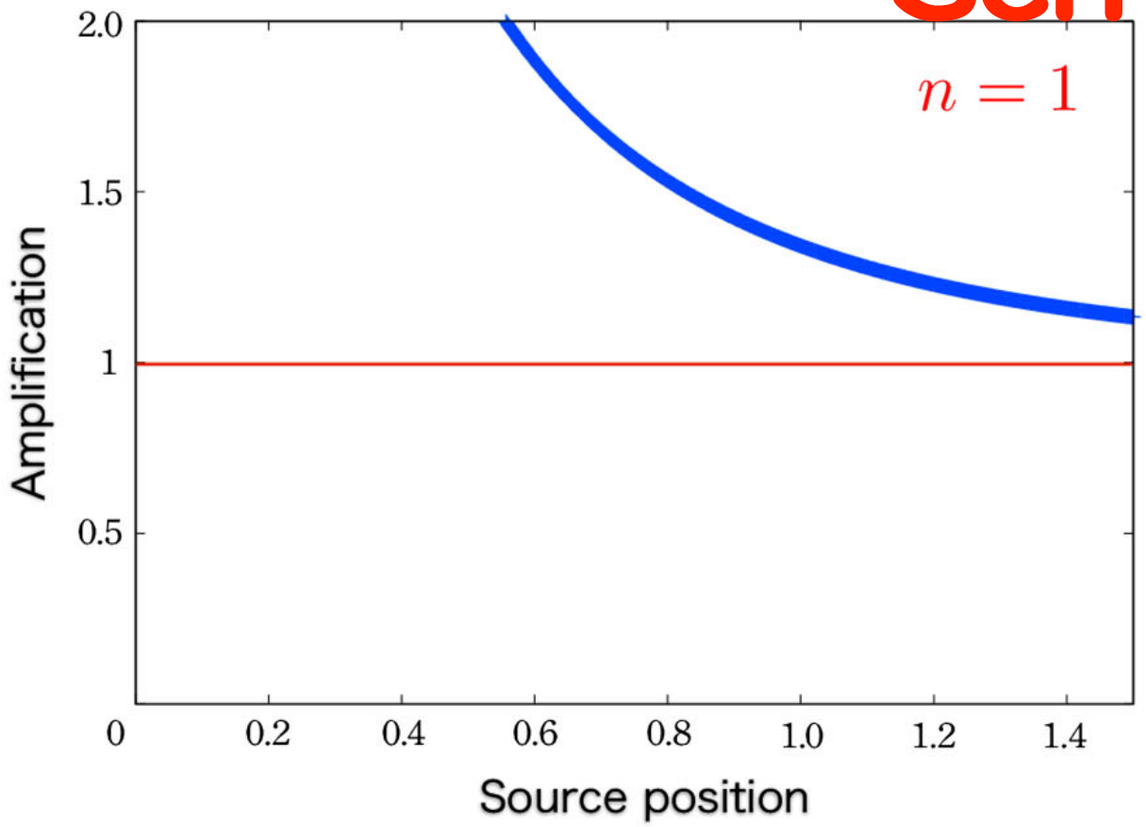
$n = 1$
Amplification
Source position
2.0
1.5
1
0.5
0
0.2
0.4
0.6
0.8
1.0
1.2
1.4

EWH

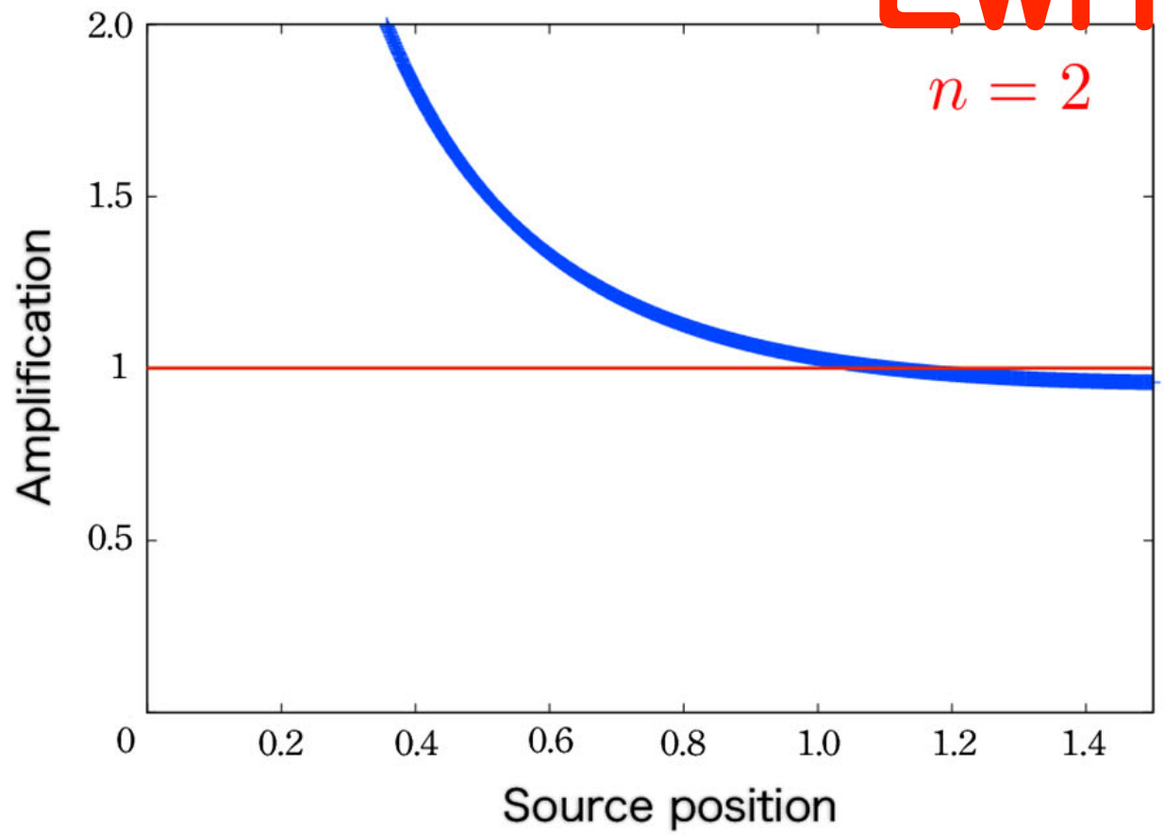
$n = 2$
Amplification
Source position
2.0
1.5
1
0.5
0
0.2
0.4
0.6
0.8
1.0
1.2
1.4

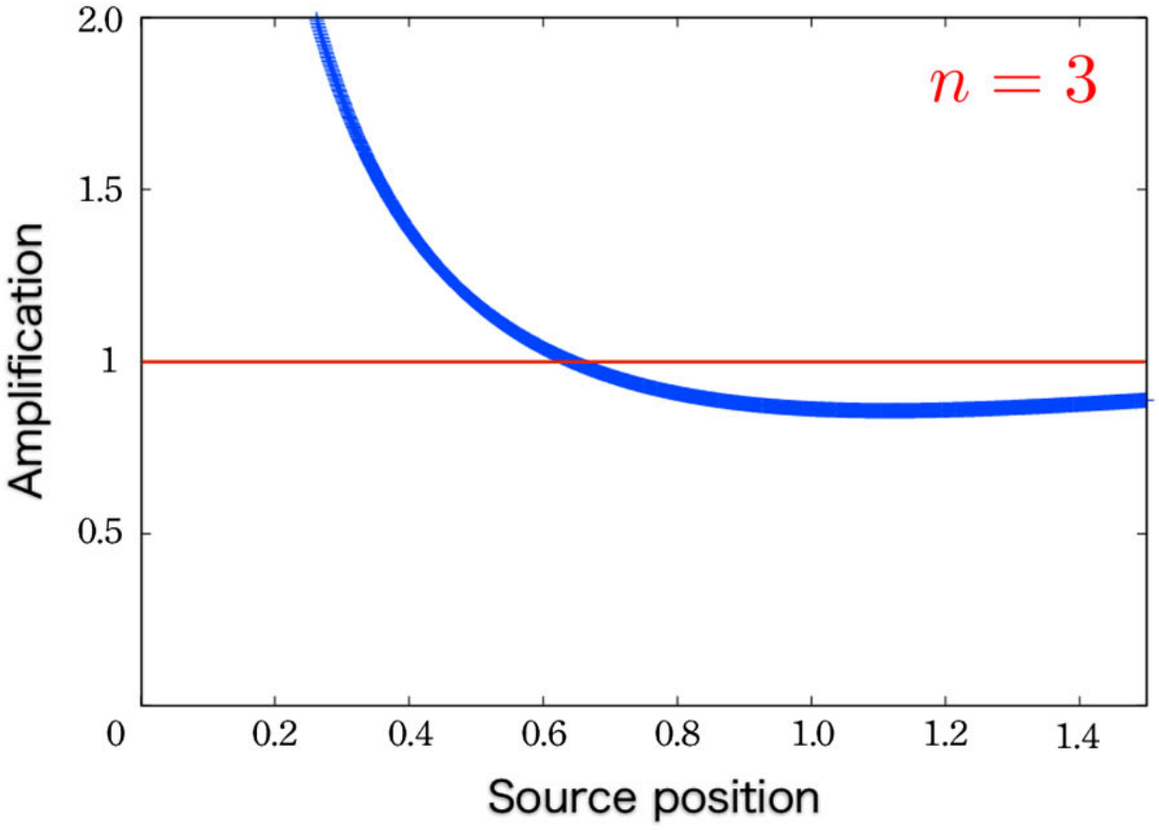
$n = 3$
Amplification
Source position
2.0
1.5
1
0.5
0
0.2
0.4
0.6
0.8
1.0
1.2
1.4

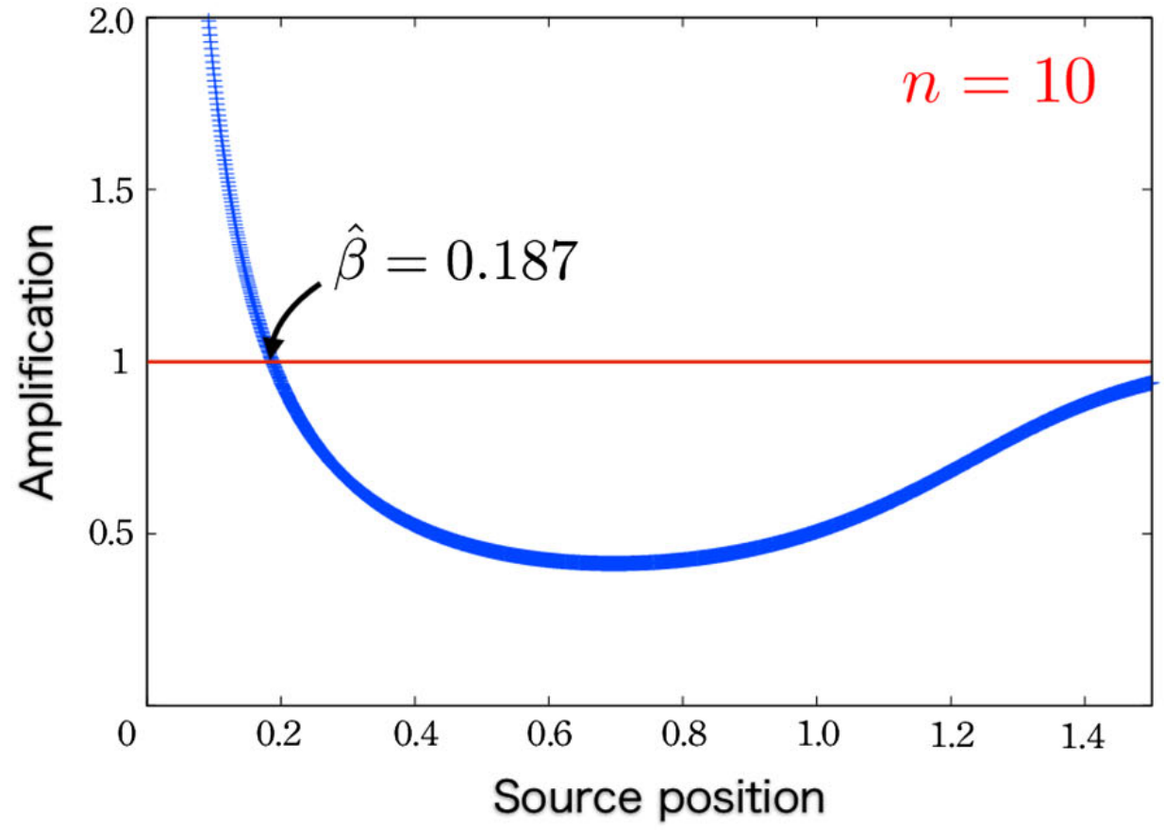
$n = 10$
$\hat{\beta} = 0.187$
Amplification
Source position
2.0
1.5
1
0.5
0
0.2
0.4
0.6
0.8
1.0
1.2
1.4

Sch

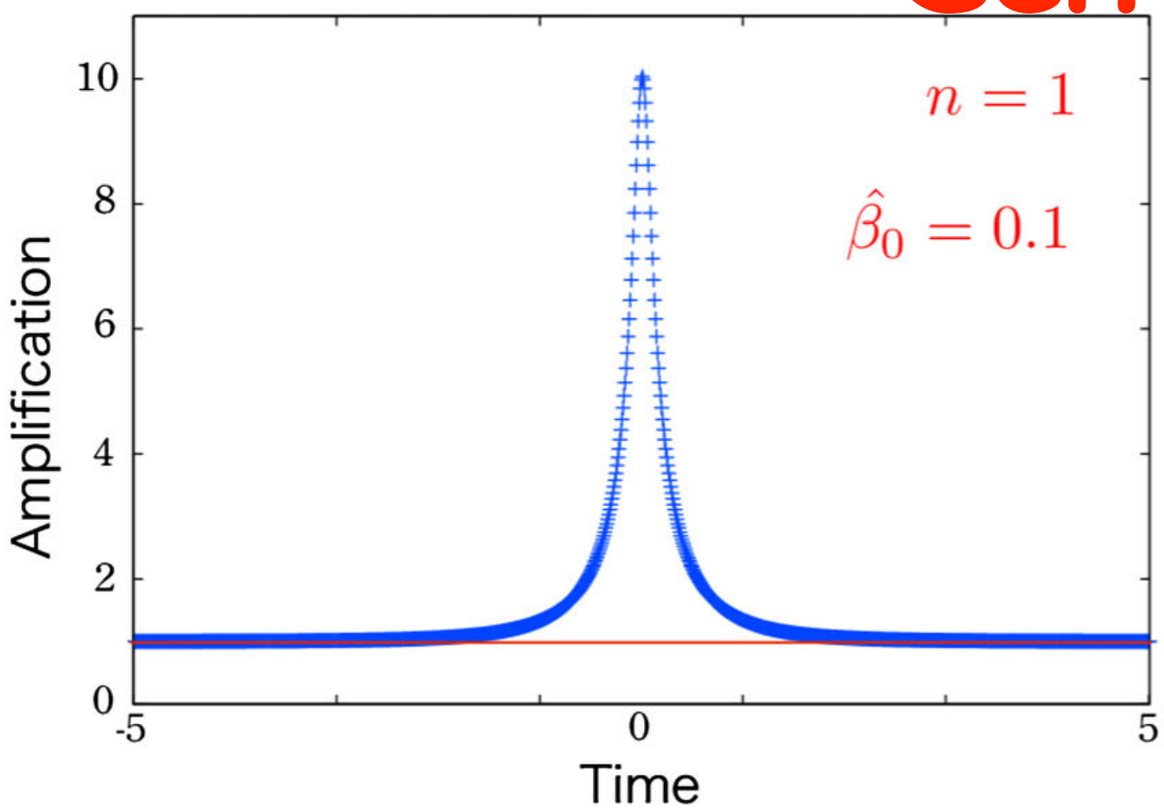
$n = 1$
$\hat{\beta}_0 = 0.1$
Amplification
Time
0
2
4
6
8
10
-5
0
5

EWH

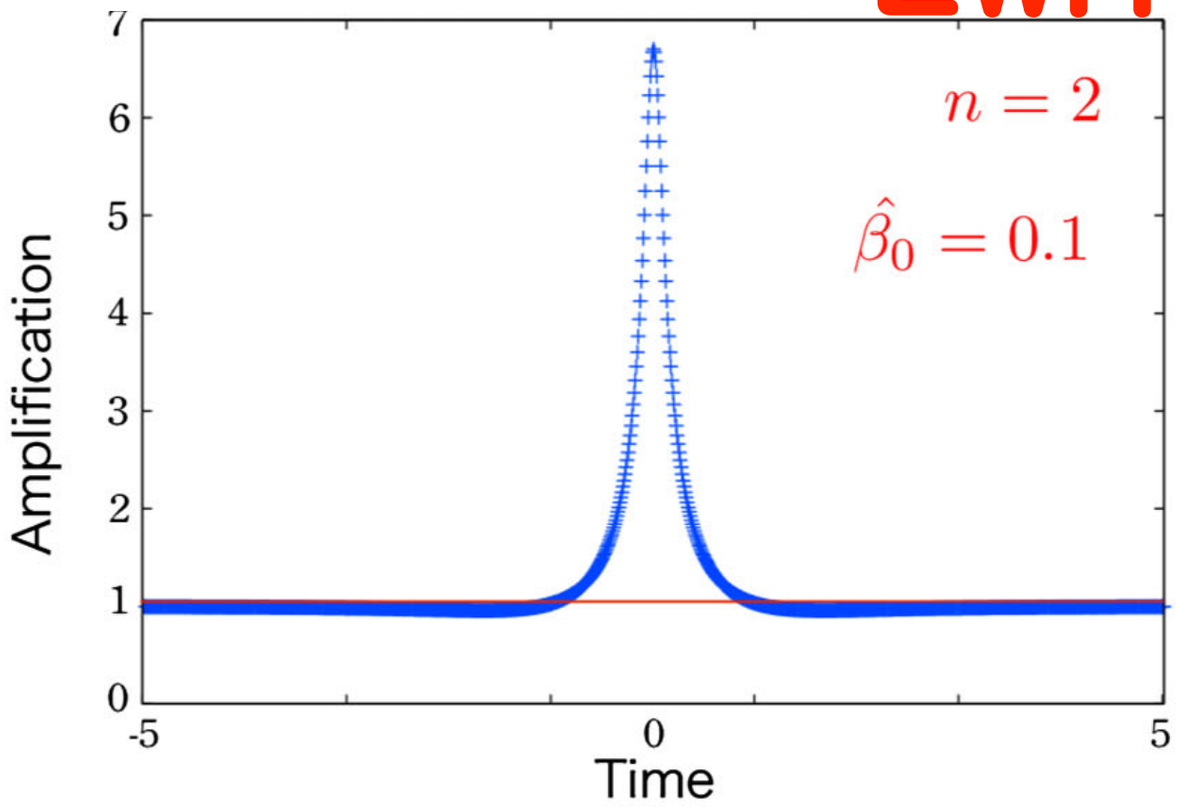
$n = 2$
$\hat{\beta}_0 = 0.1$
Amplification
Time
0
1
2
3
4
5
6
7
-5
0
5

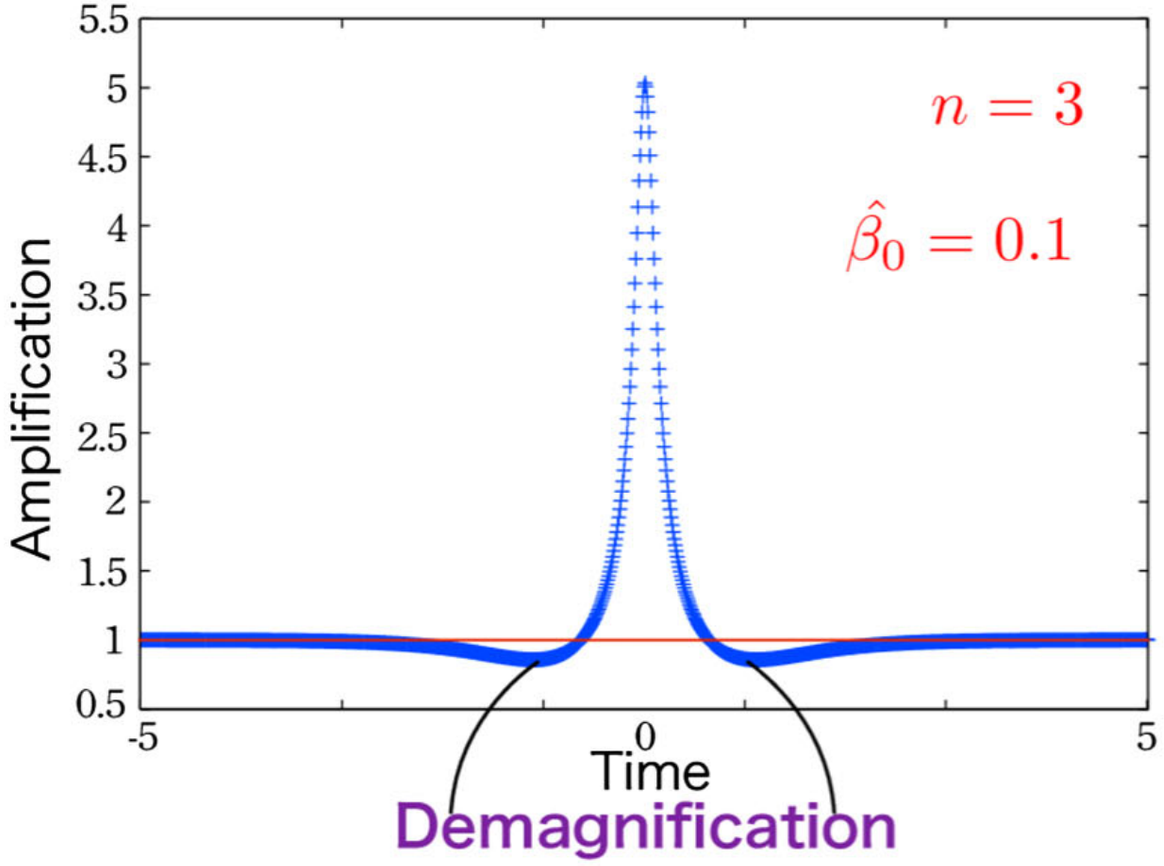
$n = 3$
$\hat{\beta}_0 = 0.1$
Amplification
Time
Demagnification
0.5
1
1.5
2
2.5
3
3.5
4
4.5
5
5.5
-5
0
5

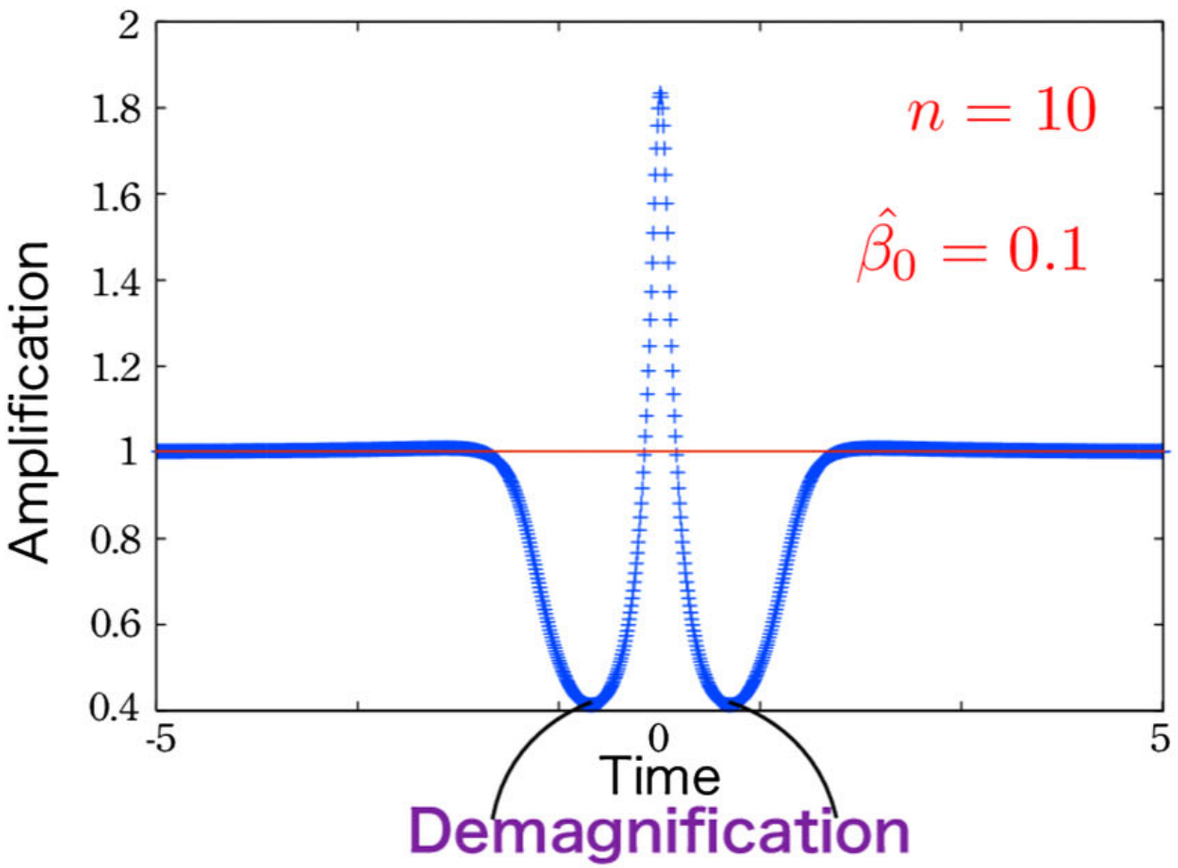
$n = 10$
$\hat{\beta}_0 = 0.1$
Amplification
Time
Demagnification
0.4
0.6
0.8
1
1.2
1.4
1.6
1.8
2
-5
0
5

Time-symmetric demagnification parts in light curves can be an evidence for EWH (n=2) but not a proof for it.

Image shape(macro)

PHYSICAL REVIEW D **88,** 024049 (2013)

Gravitational lensing shear by an exotic lens object with negative convergence or negative mass

Koji Izumi, Chisaki Hagiwara, Koki Nakajima, Takao Kitamura, and Hideki Asada
Faculty of Science and Technology, Hirosaki University, Hirosaki 036-8561, Japan
(Received 22 May 2013; published 29 July 2013)

2D-vectorial equations

A. $\varepsilon > 0$ case

$$\hat{\boldsymbol{\beta}} = \hat{\boldsymbol{\theta}} - \frac{\hat{\boldsymbol{\theta}}}{\hat{\theta}^{n+1}} \quad (\hat{\theta} > 0),$$

$$\hat{\boldsymbol{\beta}} = \hat{\boldsymbol{\theta}} - \frac{\hat{\boldsymbol{\theta}}}{(-\hat{\theta})^{n+1}} \quad (\hat{\theta} < 0),$$

magnification matrix $A_{ij} \equiv \partial \beta^i / \partial \theta_j$

$$(A_{ij}) = \begin{pmatrix} 1 - \frac{1}{\hat{\theta}^{n+1}} + (n+1)\frac{\hat{\theta}_x \hat{\theta}_x}{\hat{\theta}^{n+3}} & (n+1)\frac{\hat{\theta}_x \hat{\theta}_y}{\hat{\theta}^{n+3}} \\ (n+1)\frac{\hat{\theta}_x \hat{\theta}_y}{\hat{\theta}^{n+3}} & 1 - \frac{1}{\hat{\theta}^{n+1}} + (n+1)\frac{\hat{\theta}_y \hat{\theta}_y}{\hat{\theta}^{n+3}} \end{pmatrix}.$$

for $\hat{\theta} > 0$

Axisymmetry enables to diagonalise the magnification matrix as

$$(A_{ij}) = \begin{pmatrix} 1-\kappa-\gamma & 0 \\ 0 & 1-\kappa+\gamma \end{pmatrix} \equiv \begin{pmatrix} \lambda_- & 0 \\ 0 & \lambda_+ \end{pmatrix},$$

$$\lambda_+ = \frac{\beta}{\hat{\theta}} = 1 - \frac{1}{\hat{\theta}^{n+1}},$$

$$\lambda_- = \frac{d\hat{\beta}}{d\hat{\theta}} = 1 + \frac{n}{\hat{\theta}^{n+1}}.$$

$$\text{convergence} \quad \kappa = 1 - \frac{\lambda_+ + \lambda_-}{2} = \frac{1-n}{2}\,\frac{1}{\hat{\theta}^{n+1}},$$

$$\text{shear} \quad \gamma = \frac{\lambda_+ - \lambda_-}{2} = -\frac{1+n}{2}\,\frac{1}{\hat{\theta}^{n+1}},$$

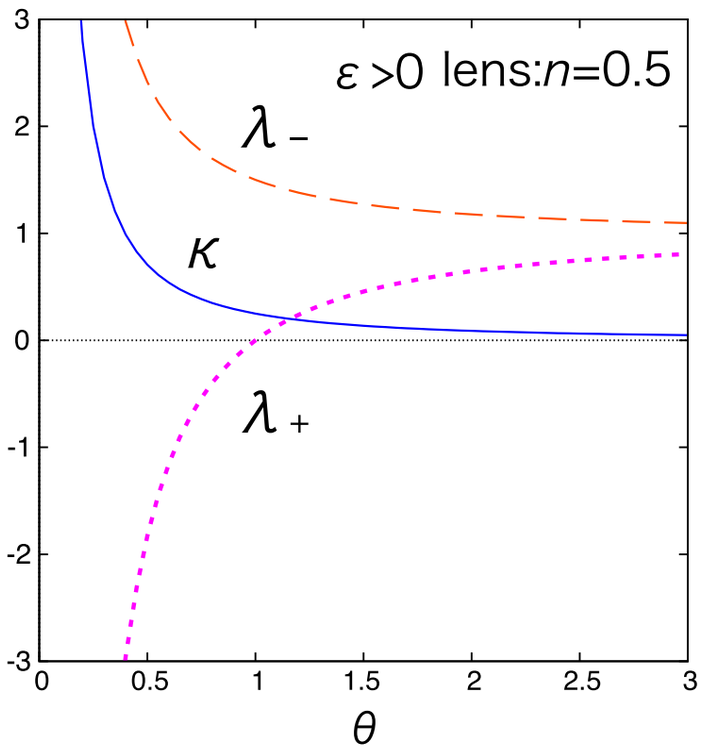

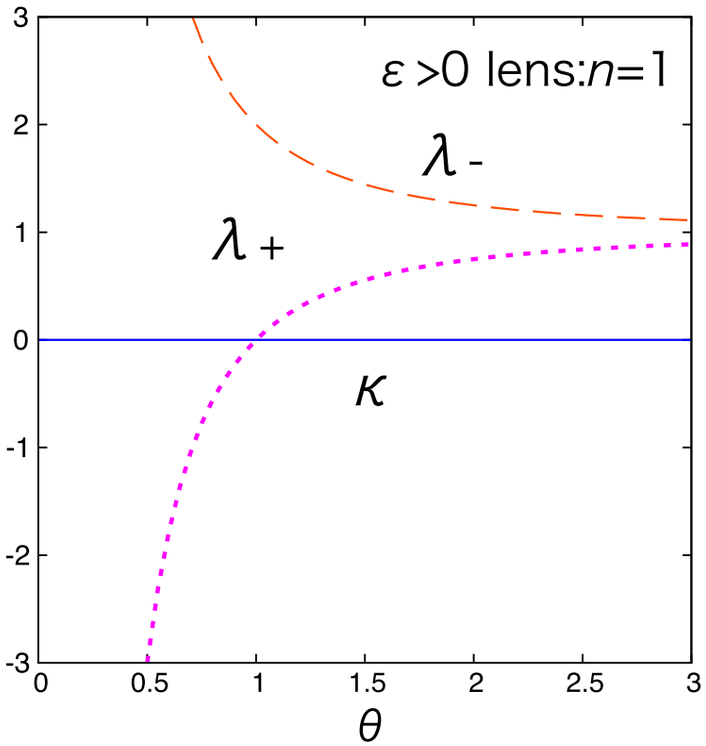

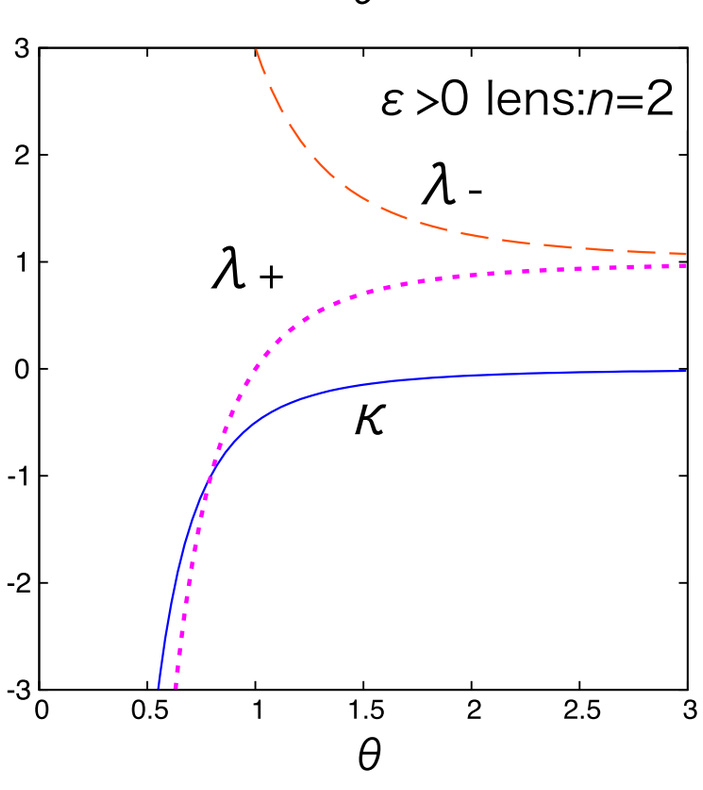

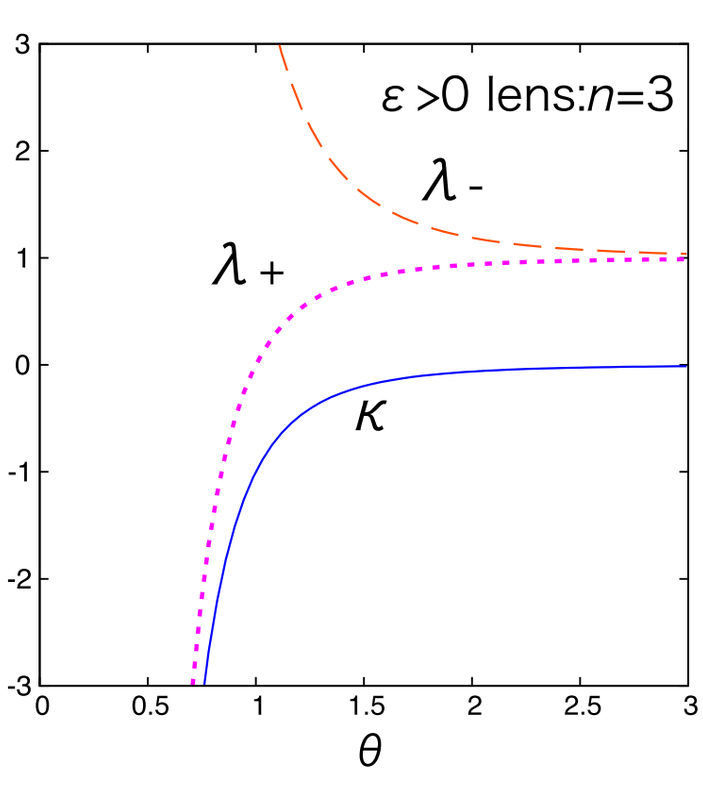

$\lambda_- > \lambda_+$ **tangentially elongated**

B. $\varepsilon < 0$ case

$$\hat{\boldsymbol{\beta}} = \hat{\boldsymbol{\theta}} + \frac{\hat{\boldsymbol{\theta}}}{\hat{\theta}^{n+1}} \quad (\hat{\theta} > 0),$$

repulsive

like a concave lens

$$\hat{\boldsymbol{\beta}} = \hat{\boldsymbol{\theta}} + \frac{\hat{\boldsymbol{\theta}}}{(-\hat{\theta})^{n+1}} \quad (\hat{\theta} < 0).$$

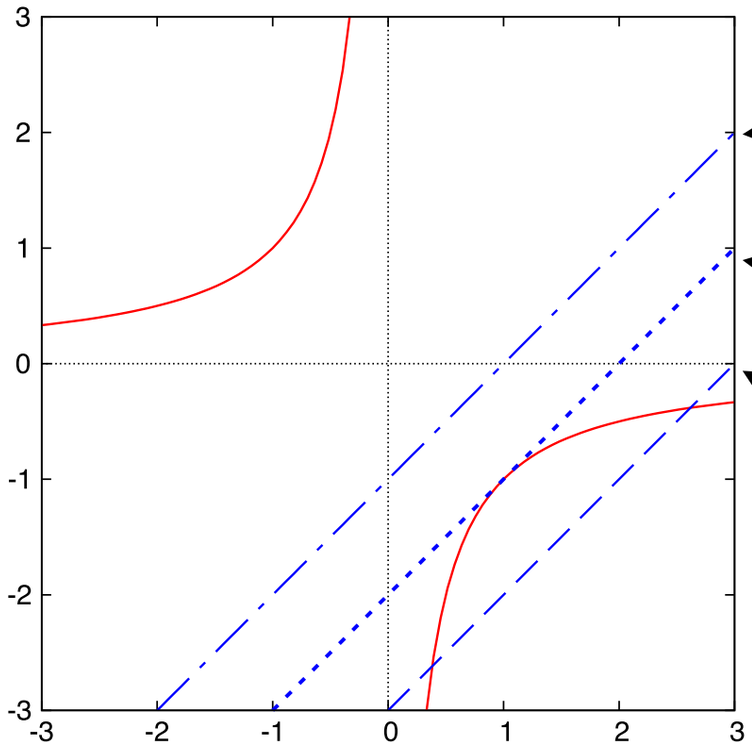

0 images

1 images

2 images

FIG. 3 (color online). Repulsive lens model ($\varepsilon < 0$). Solid curves denote $1/\hat{\theta}^n$ and straight lines mean $\hat{\theta} - \hat{\beta}$. Their intersections correspond to image positions that are roots for the lens equation. There are three cases: No image for a small $\hat{\beta}$ (dot-dashed line), a single image for a particular $\hat{\beta}$ (dotted line), and two images for a large $\hat{\beta}$ (dashed line). The two images are on the same side of the lens object.

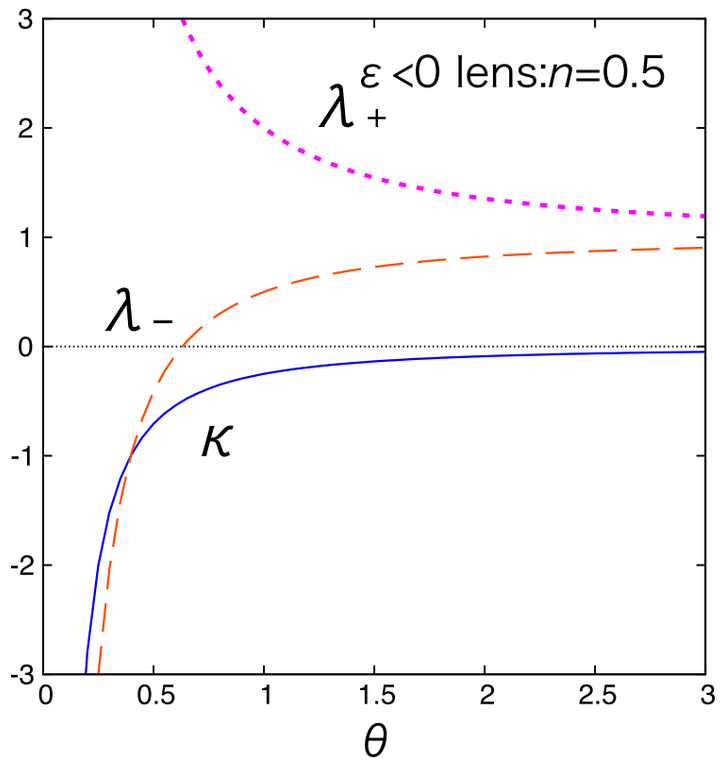

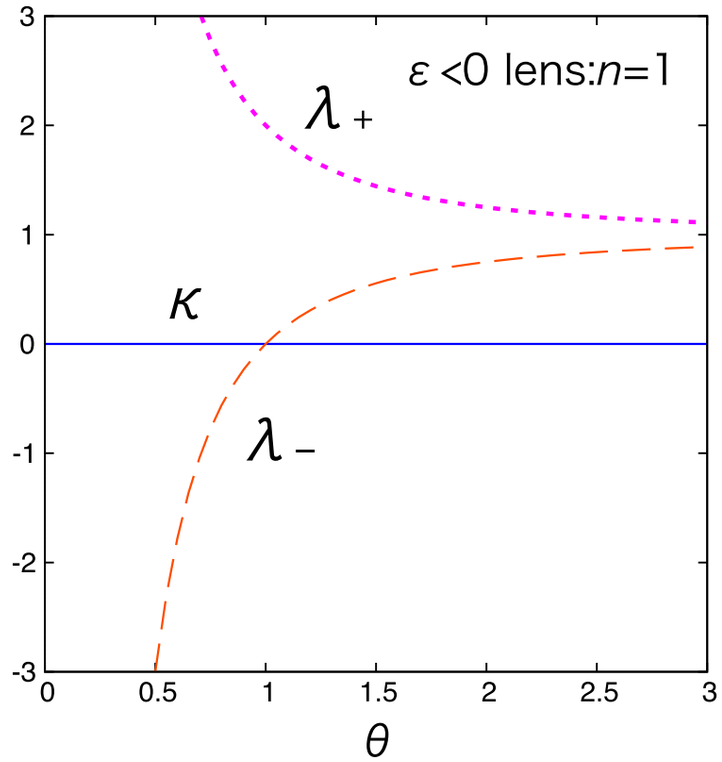

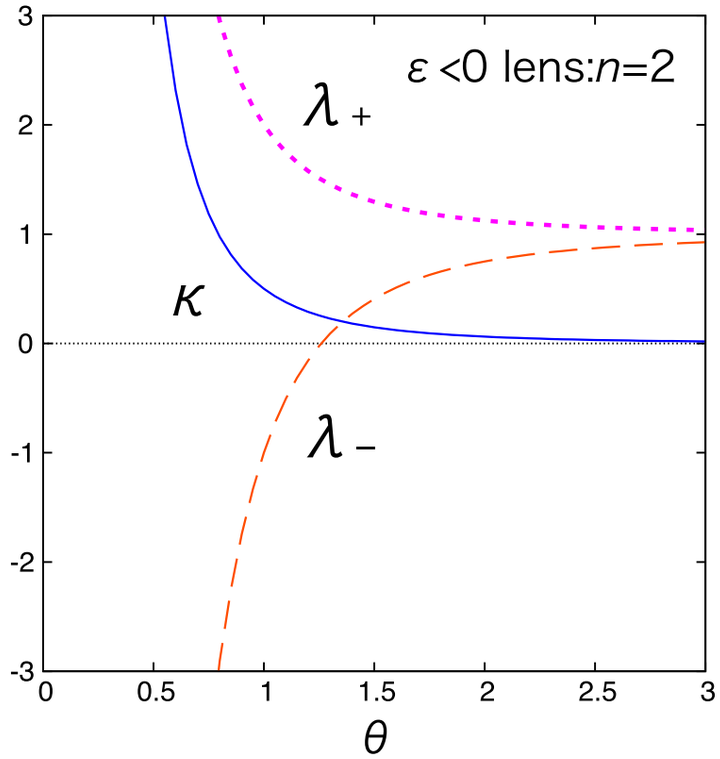

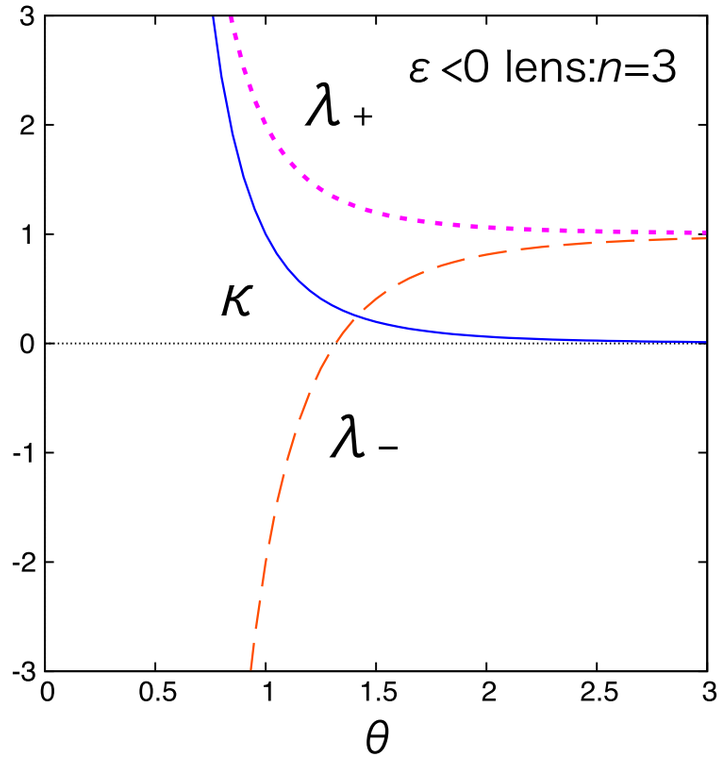

$\lambda_- < \lambda_+$

radially elongated

Numerical images

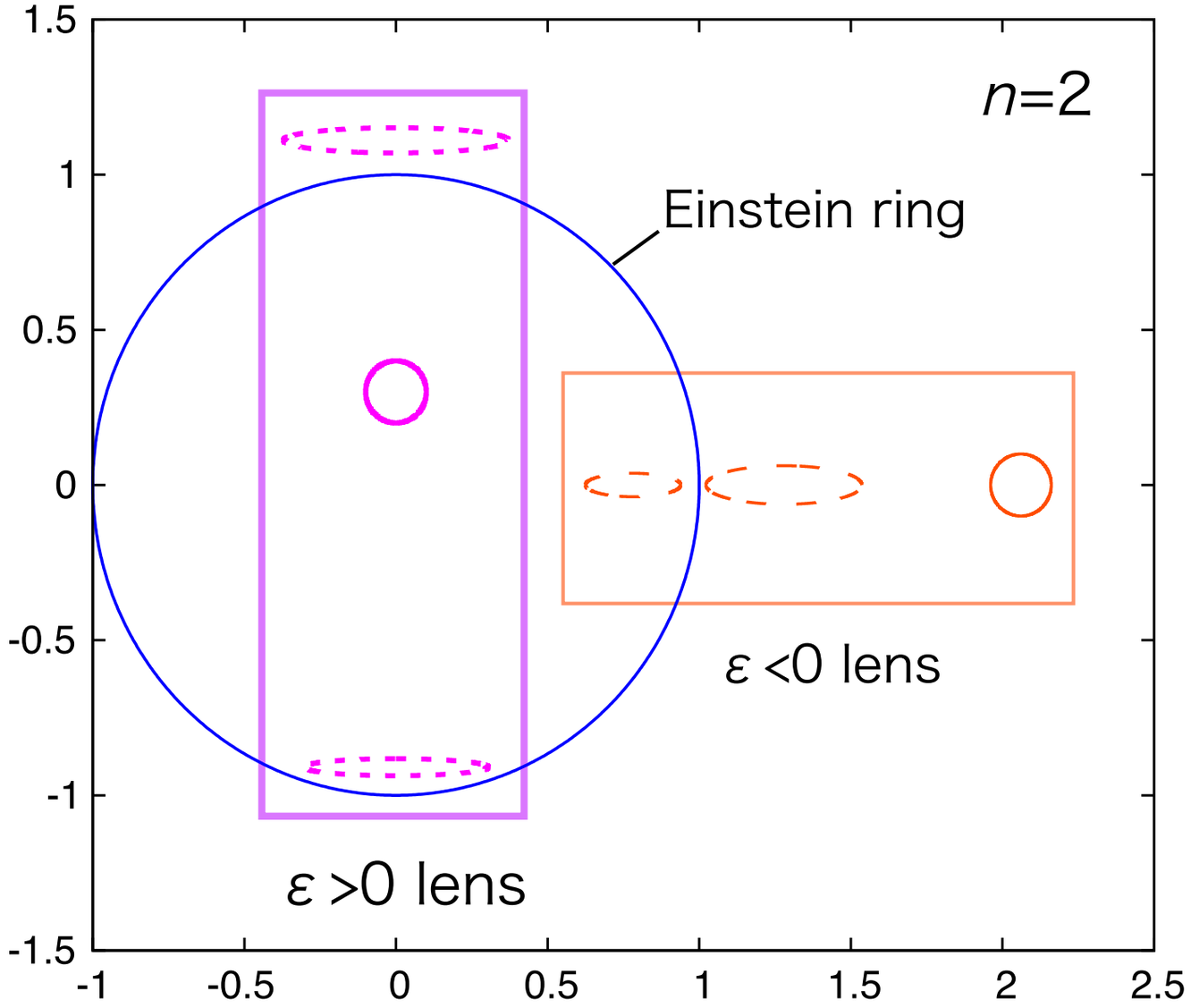

FIG. 2 (color online). Numerical figures of lensed images for attractive ($\varepsilon > 0$) and repulsive ($\varepsilon < 0$) cases. They are denoted by dashed curves. We take $n = 2$. The source for each case is denoted by solid circles, which are located on the horizontal axis and the vertical one for $\varepsilon < 0$ and $\varepsilon > 0$, respectively.

No lens

M > 0

M < 0

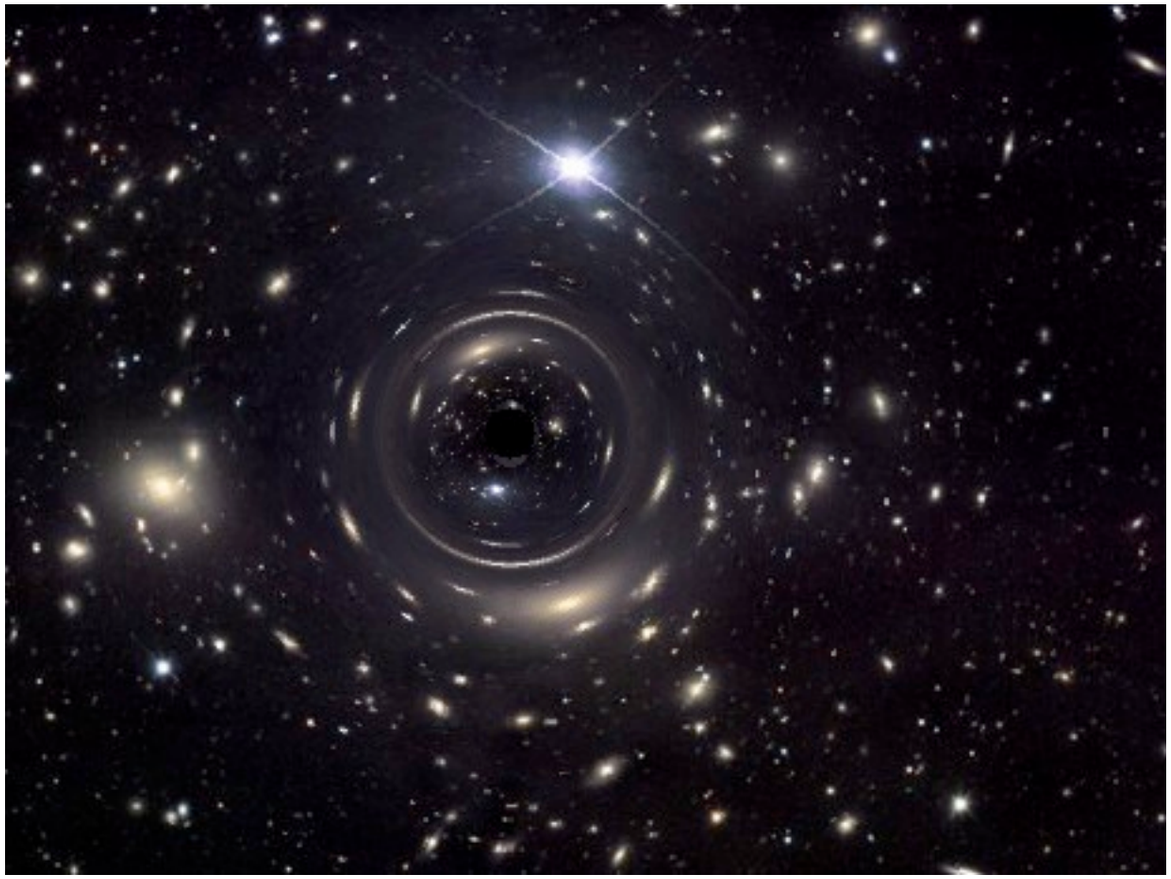

courtesy of Koji Izumi

Application to cosmology

Cosmic voids: effective $\kappa < 0$

Y. Higuchi, M. Oguri and T. Hamana, MNRAS (2013)

"Measuring the mass distribution of voids with stacked weak lensing"

Numerical simulations for near-future surveys

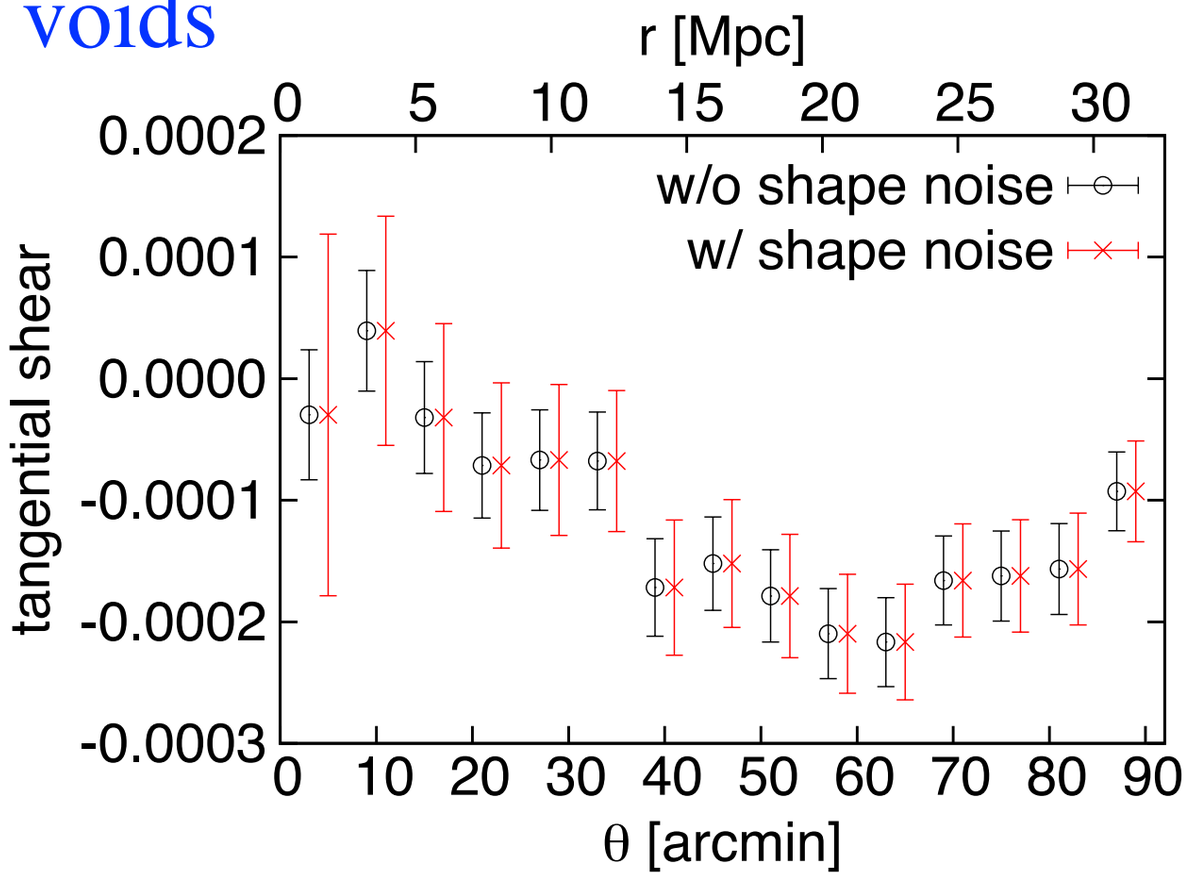

"First measurement of gravitational lensing by cosmic voids in SDSS", Melchior et al., ArXiv:1309.2045

Image motion(micro)

Microlensed image centroid motions by an exotic lens object with negative convergence or negative mass

Takao Kitamura, Koji Izumi, Koki Nakajima, Chisaki Hagiwara, and Hideki Asada

Faculty of Science and Technology,

Hirosaki University, Hirosaki 036-8561, Japan

(Dated: July 25, 2013)

ArXiv:1307.6637

Microlensing observables in astrometry such as Gaia and JASMINE are

the centroid position of the light distribution

$$\hat{\boldsymbol{\theta}}_{pc} = \frac{A_1\boldsymbol{\theta}_1 + A_2\boldsymbol{\theta}_2}{A_{tot}},$$

The relative displacement of the image centroid with respect to the source position

$$\delta\hat{\boldsymbol{\theta}}_{pc} = \hat{\boldsymbol{\theta}}_{pc} - \hat{\boldsymbol{\beta}}.$$

Many works for Sch and Binary Lens

M. A. Walker, Astrophys. J. **453**, 37 (1995).

M. Miyamoto, and Y. Yoshii, Astron. J. **110**, 1427 (1995).

M. Hosokawa, K. Ohnishi, and T. Fukushima, Astron. J. **114**, 1508 (1997).

N. Safizadeh, N. Dalal, and K. Griest, Astrophys. J. **522**, 512 (1999).

Y. Jeong, C. Han, and S. Park, Astrophys. J. **511**, 569 (1999).

G. F. Lewis, X. R. Wang, Prog. Theor. Phys. **105**, 893 (2001).

H. Asada, Astrophys. J. **573**, 825 (2002).

C. Han, and C. Lee, Mon. Not. Roy. Astron. Soc. **329**, 163 (2002).

EWH case

Y. Toki, T. Kitamura, H. Asada, and F. Abe, Astrophys. J. **740**, 121 (2011).

Convex-type

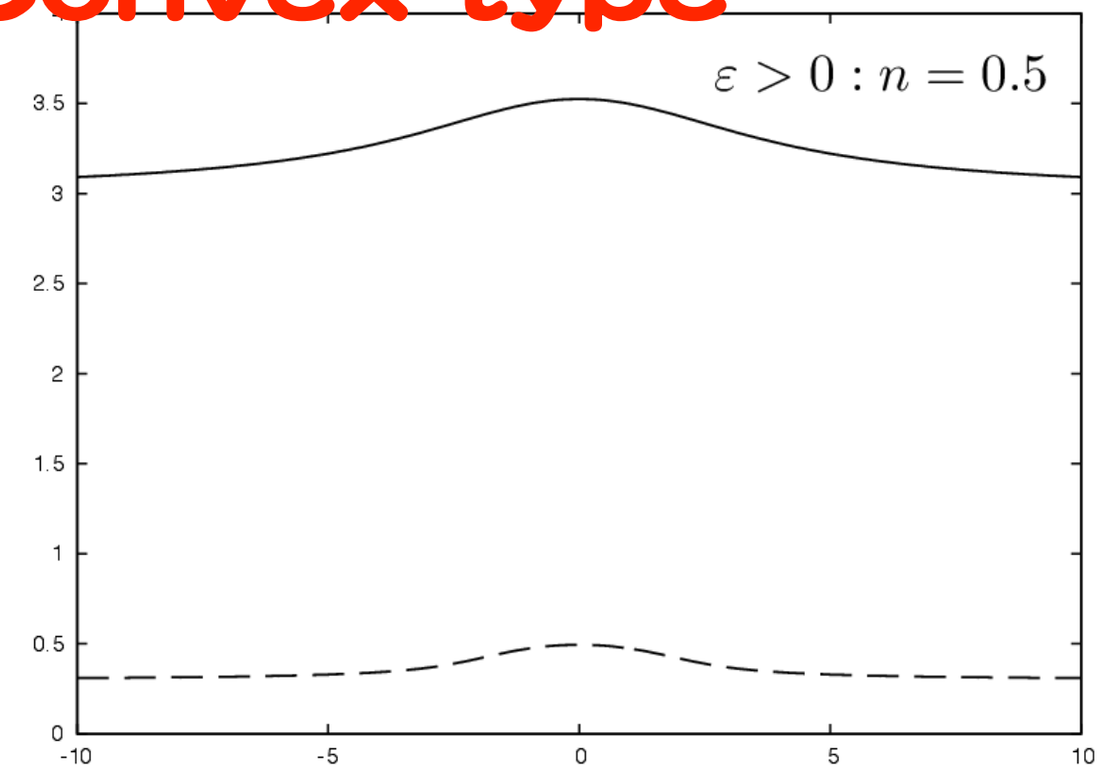

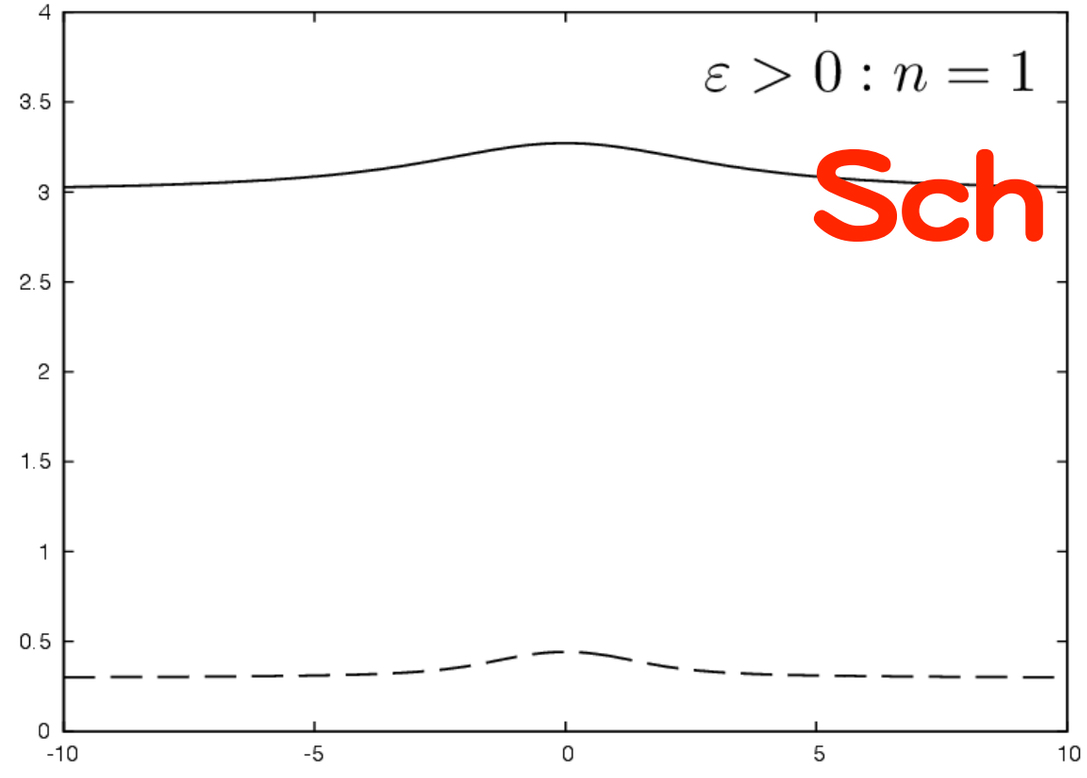

Sch

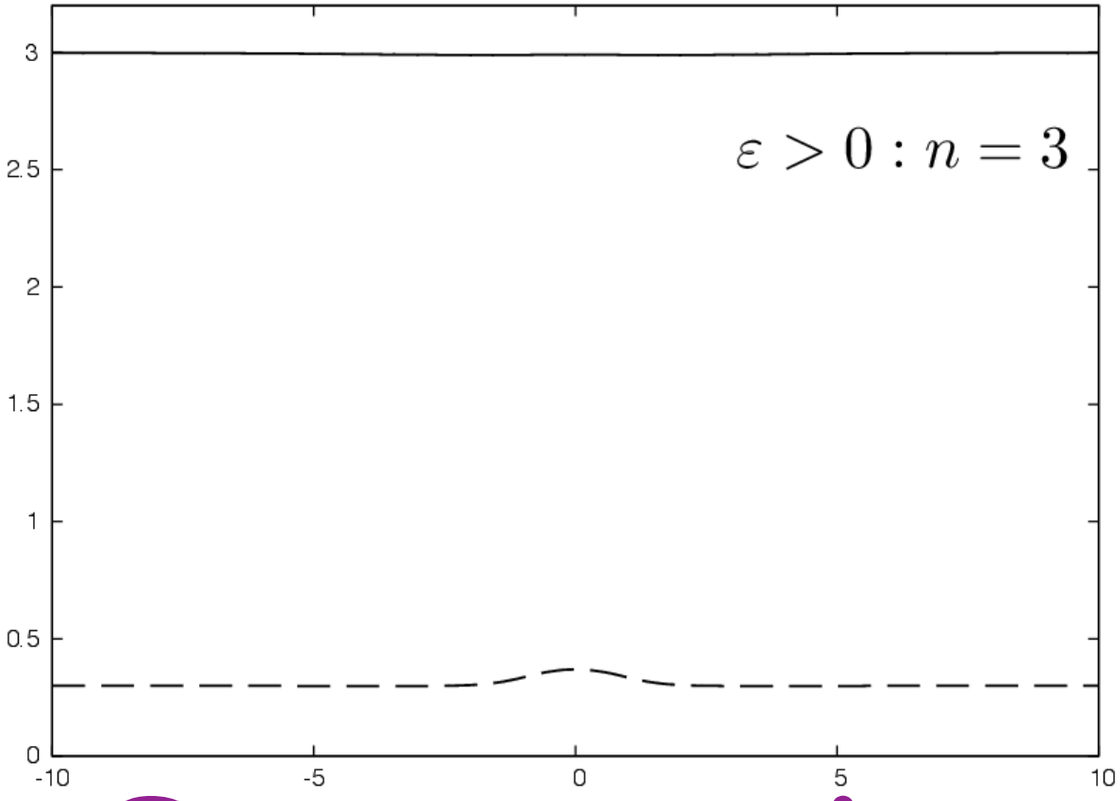

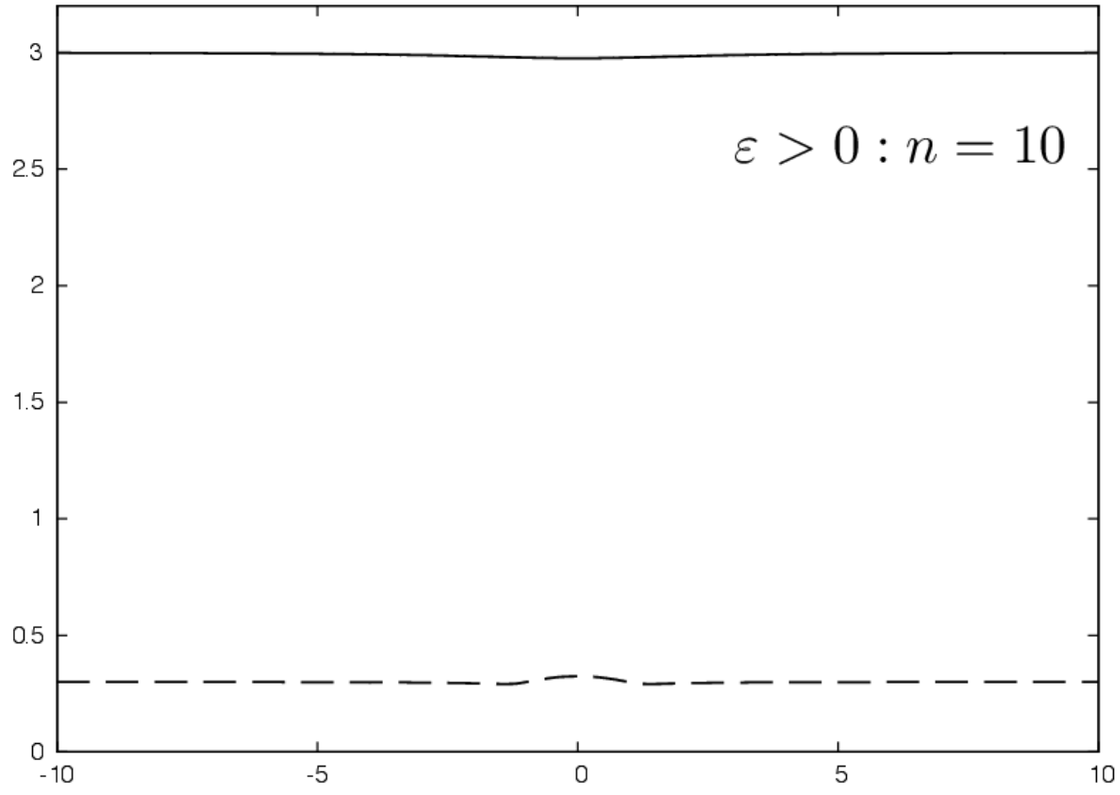

Source motion

Convex-type

Sch

Trajectry becomes multiply-connected only for n>3

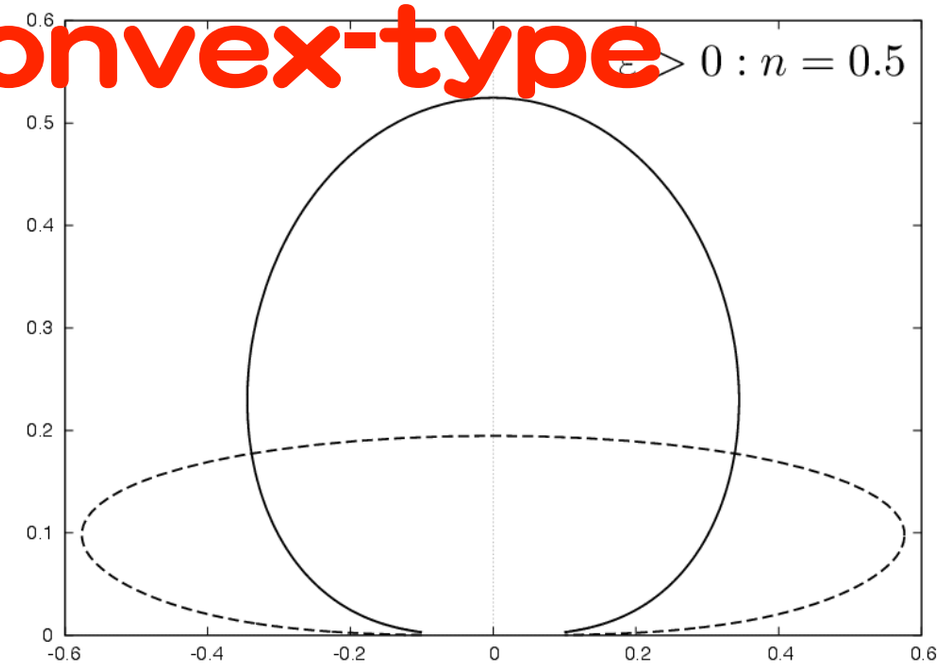

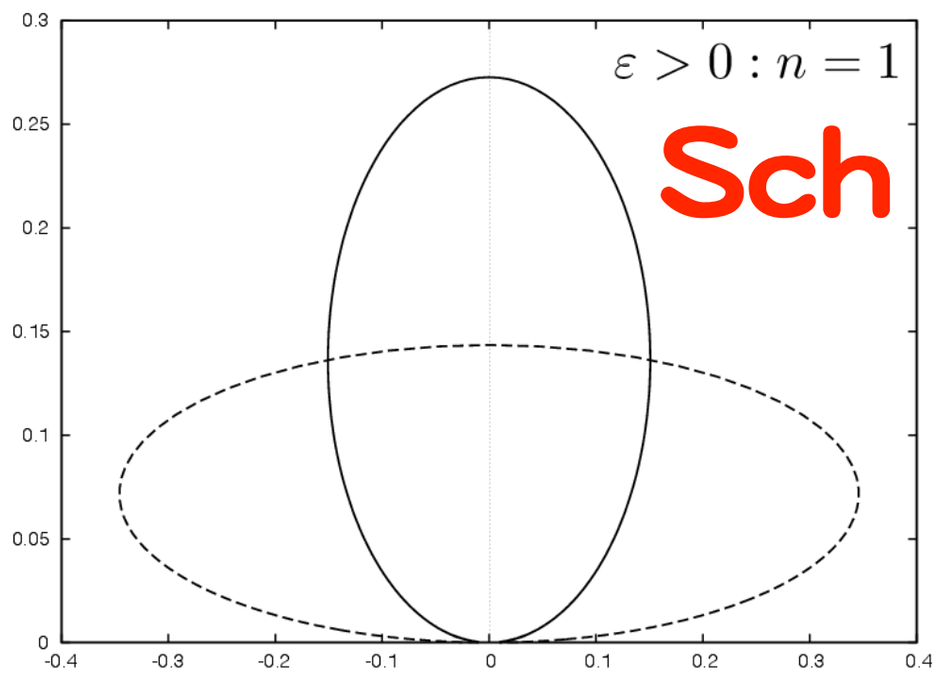

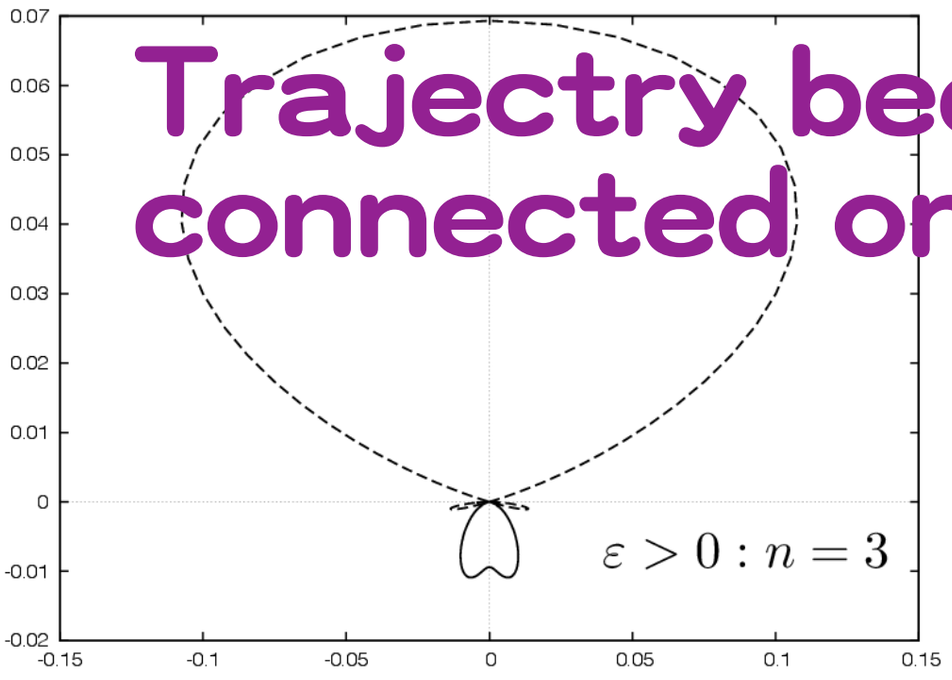

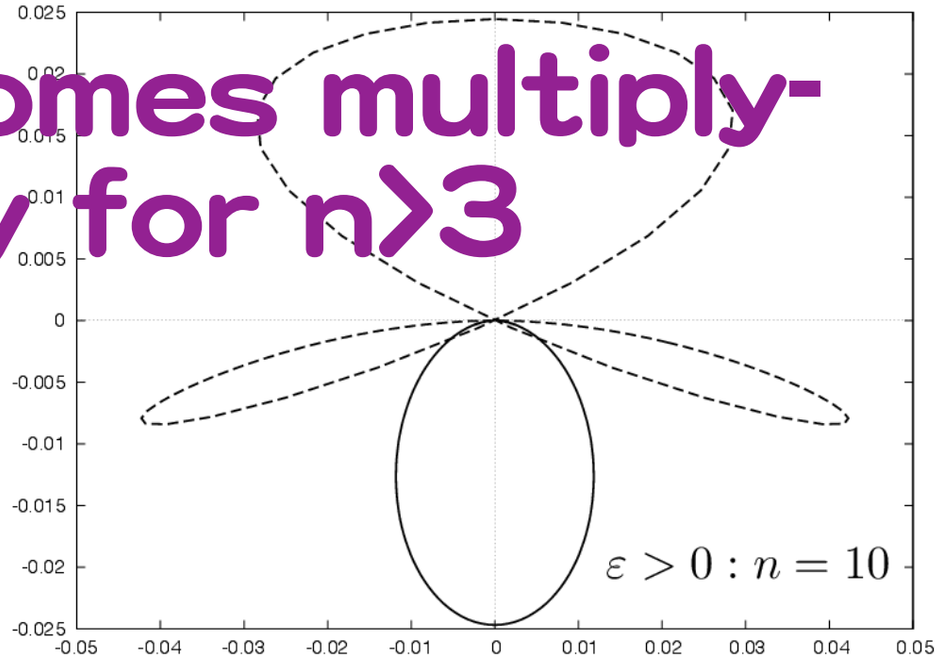

FIG. 3: Centroid shifts $\delta\hat{\boldsymbol{\theta}}_{pc}$ for $\varepsilon > 0$ (convex-type attractive models). The solid and dashed curves correspond to $\hat{\beta}_0 = 3$ and $\hat{\beta}_0 = 0.3$, respectively. The horizontal axis along the source velocity is $\delta\hat{\theta}_{pc,x}$ and the vertical axis is $\delta\hat{\theta}_{pc,y}$. Top left: $n = 0.5$ Top right: $n = 1$. Bottom left: $n = 3$. Bottom right: $n = 10$.

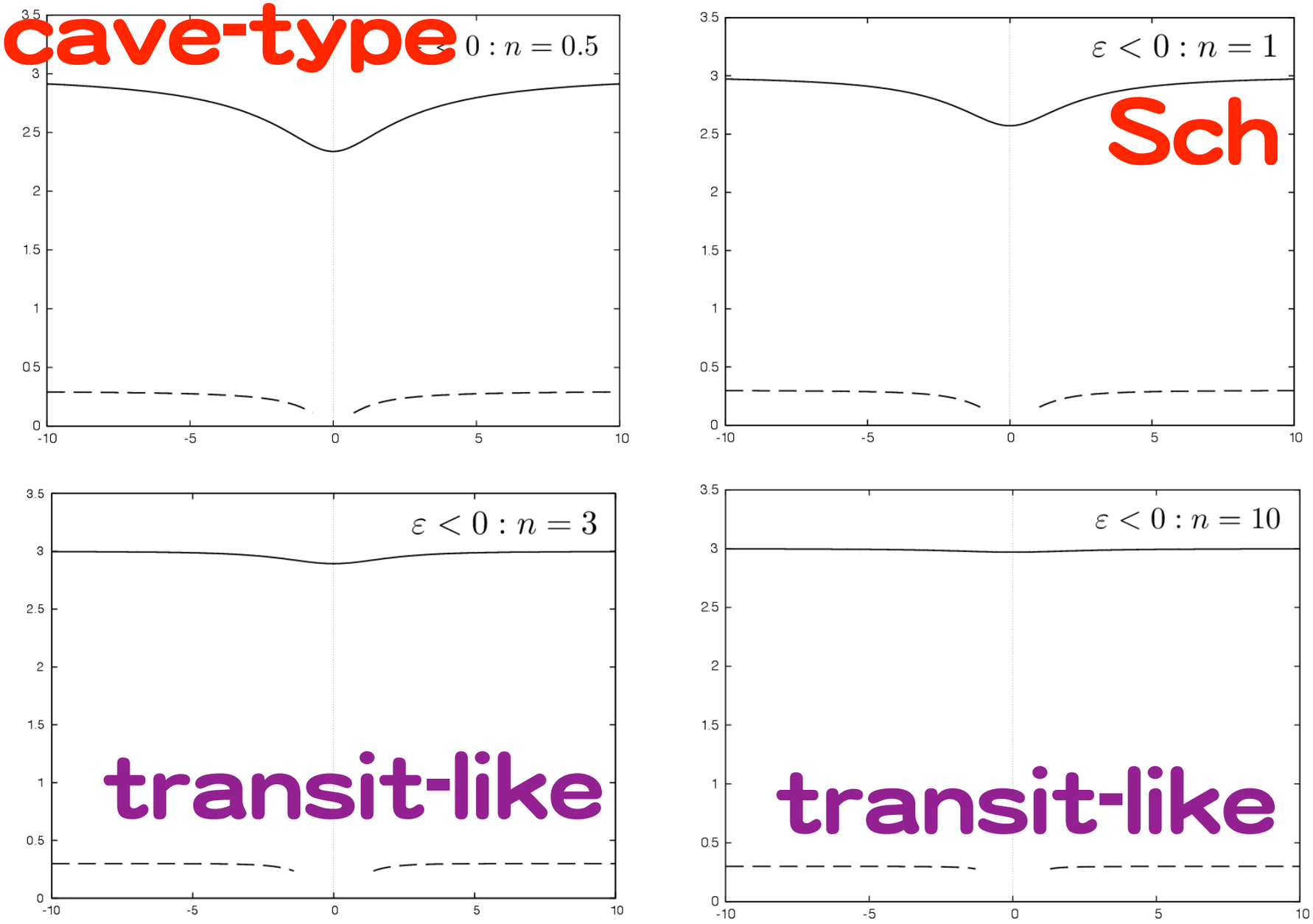

FIG. 6: Centroid motions as $(\hat{\theta}_{pc,x}, \hat{\theta}_{pc,y})$ for $\varepsilon < 0$ (repulsive models). The solid and dashed curves correspond to $\hat{\beta}_0 = 3$ and $\hat{\beta}_0 = 0.3$, respectively. The horizontal axis along the source linear motion is $\hat{\theta}_{pc,x}$ and the vertical axis is $\hat{\theta}_{pc,y}$. The dashed curves do not exist for small $\hat{\beta}$, where no images appear. Top left: $n = 0.5$ Top right: $n = 1$. Bottom left: $n = 3$. Bottom right: $n = 10$.

Concave-type

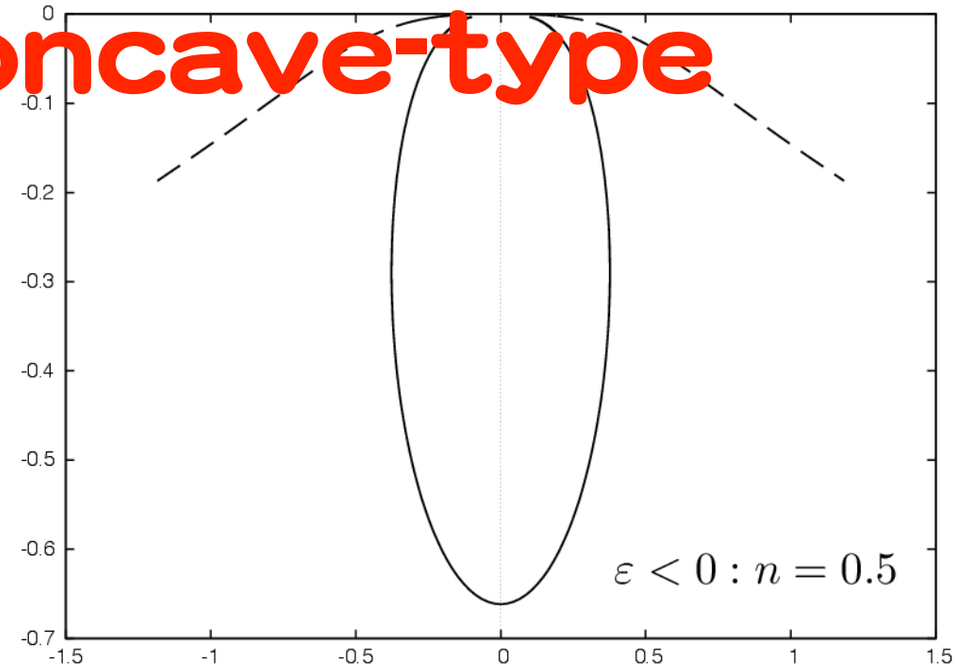

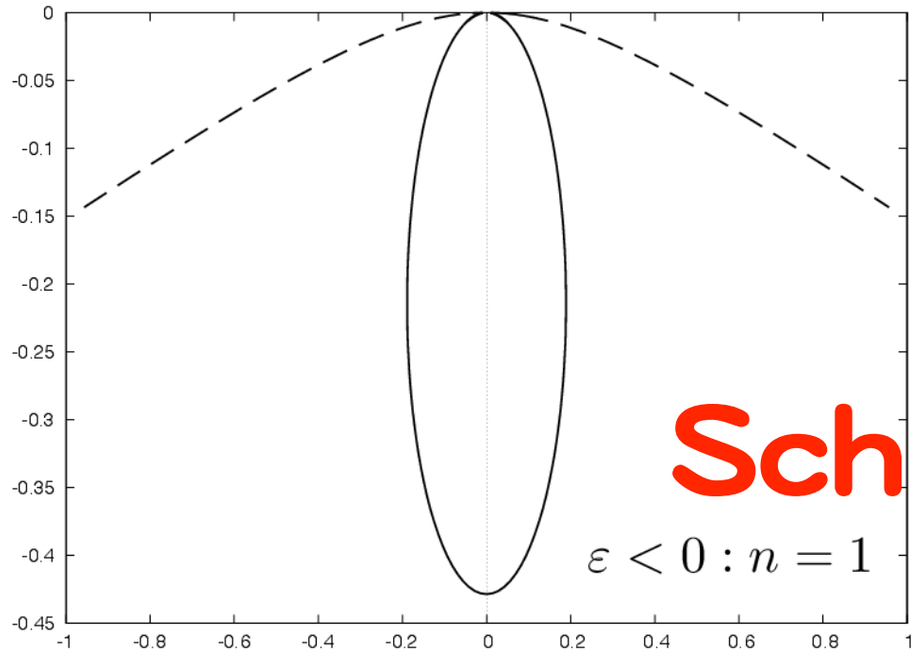

Sch

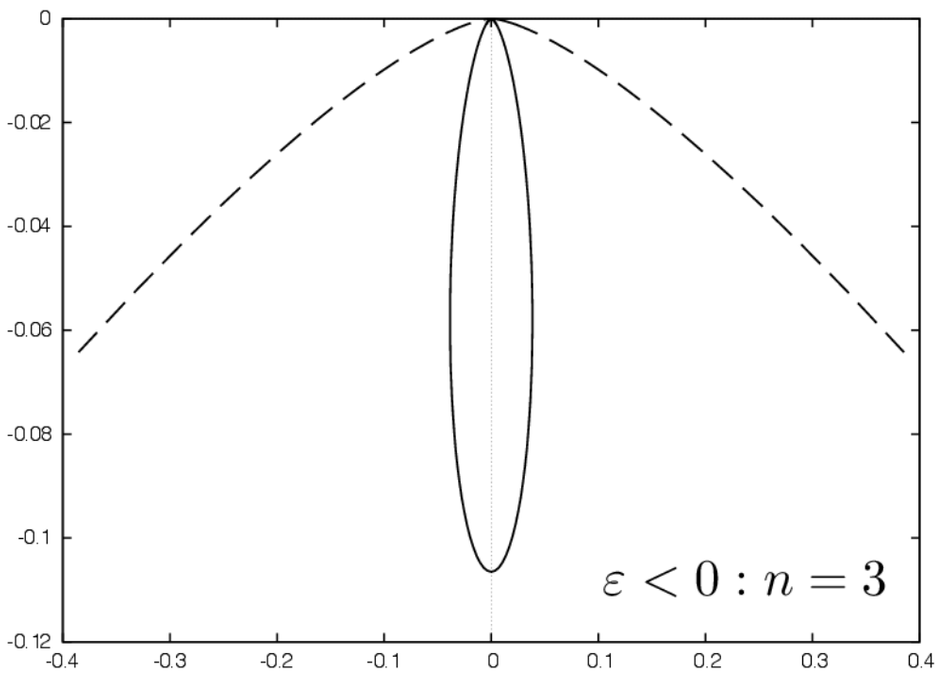

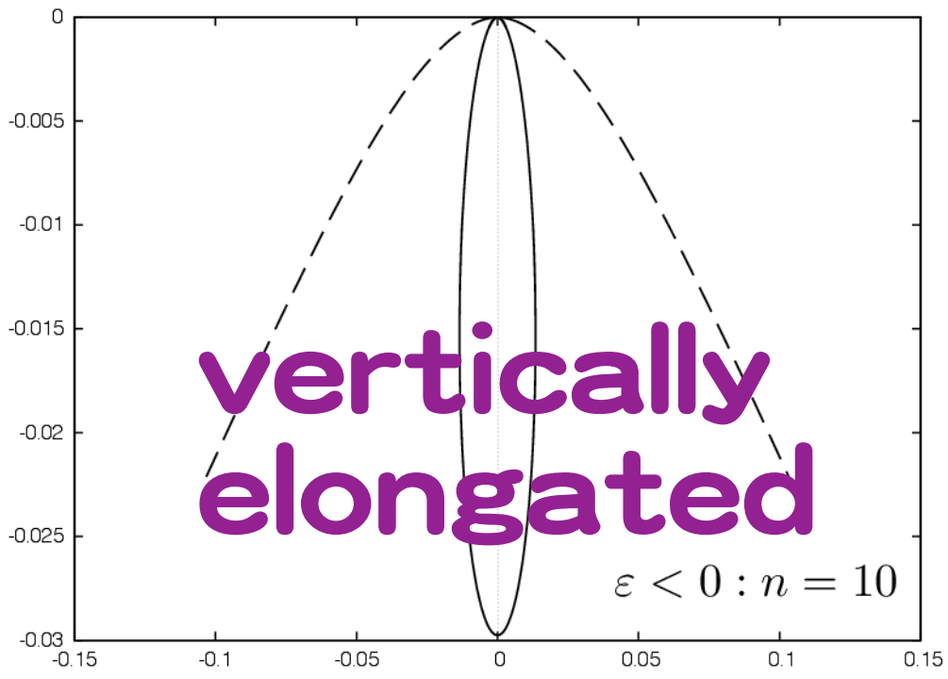

FIG. 7: Centroid shifts $\delta\hat{\boldsymbol{\theta}}_{pc}$ for $\varepsilon < 0$ (concave-type repulsive models). The solid and dashed curves correspond to $\hat{\beta}_0 = 3$ and $\hat{\beta}_0 = 0.3$, respectively. The horizontal axis along the source velocity is $\delta\hat{\theta}_{pc,x}$ and the vertical axis is $\delta\hat{\theta}_{pc,y}$. The dashed curves are not closed, because no images appear for small $\hat{\beta}$. Top left: $n = 0.5$ Top right: $n = 1$. Bottom left: $n = 3$. Bottom right: $n = 10$.

Concluding remarks

Exotic lens models suggest
unusual observational features.

They might be used
for searching (or constraining)
exotic matter/energy/gravity.

Dark matter and Dark energy
play a role in cosmology.

Is there another (3rd) dark component
in the universe ?

One example:

The Astrophysical Journal Letters, 768:L16 (4pp), 2013 May 1 doi:10.1088/2041-8205/768/1/L16

OBSERVATIONAL UPPER BOUND ON THE COSMIC ABUNDANCES OF NEGATIVE-MASS COMPACT OBJECTS AND ELLIS WORMHOLES FROM THE SLOAN DIGITAL SKY SURVEY QUASAR LENS SEARCH

Ryuichi Takahashi and Hideki Asada
Faculty of Science and Technology, Hirosaki University, Hirosaki 036-8561, Japan
Received 2013 March 6; accepted 2013 April 4; published 2013 April 17

ABSTRACT

The latest result in the Sloan Digital Sky Survey Quasar Lens Search (SQLS) has set the first cosmological constraints on negative-mass compact objects and Ellis wormholes. There are no multiple images lensed by the above two exotic objects for ∼50,000 distant quasars in the SQLS data. Therefore, an upper bound is put on the cosmic abundances of these lenses. The number density of negative-mass compact objects is $n < 10^{-8}(10^{-4})\,h^3\,\mathrm{Mpc}^{-3}$ at the mass scale $|M| > 10^{15}(10^{12})\,M_\odot$, which corresponds to the cosmological density parameter $|\Omega| < 10^{-4}$ at the galaxy and cluster mass range $|M| = 10^{12-15}\,M_\odot$. The number density of the Ellis wormhole is $n < 10^{-4}\,h^3\,\mathrm{Mpc}^{-3}$ for a range of the throat radius $a = 10$–10^4 pc, which is much smaller than the Einstein ring radius.

Key words: cosmology: observations – gravitational lensing: strong

negative−mass object

upper bound

$|\Omega|=1$

$|\Omega|=10^{-2}$

$|\Omega|=10^{-4}$

95%

68%

10^{5}

10^{0}

10^{-5}

n (Mpc/h)$^{-3}$

10^{10} 10^{12} 10^{14} 10^{16} 10^{18}

mass |M| ($M_\odot$/h)

Ellis wormhole

upper bound

95%

68%

10^{0}

10^{-5}

n (Mpc/h)$^{-3}$

10^{0} 10^{2} 10^{4}

throat radius a (pc/h)

Thank you !

asada@phys.hirosaki-u.ac.jp

TABLE II: Einstein radii and model parameters for Bulge and LMC lensings. θ_E is the angular Einstein radius, R_E is the Einstein radius, and $\bar{\varepsilon}$ and n are the two model parameters. $D_S = 8kpc$ and $D_L = 4kpc$ are assumed for Bulge. $D_S = 50kpc$ and $D_L = 25kpc$ are assumed for LMC.

	Bulge		LMC	
$\theta_E(mas)$	$R_E(km)$	$\frac{\bar{\varepsilon}}{R_E^n}$	$R_E(km)$	$\frac{\bar{\varepsilon}}{R_E^n}$
10^{-3}	6.0×10^5	1.0×10^{-11}	3.7×10^6	1.0×10^{-11}
10^{-2}	6.0×10^6	1.0×10^{-10}	3.7×10^7	1.0×10^{-10}
10^{-1}	6.0×10^7	1.0×10^{-9}	3.7×10^8	1.0×10^{-9}
1	6.0×10^8	1.0×10^{-8}	3.7×10^9	1.0×10^{-8}
10	6.0×10^9	1.0×10^{-7}	3.7×10^{10}	1.0×10^{-7}
10^2	6.0×10^{10}	1.0×10^{-6}	3.7×10^{11}	1.0×10^{-6}
10^3	6.0×10^{11}	1.0×10^{-5}	3.7×10^{12}	1.0×10^{-5}

TABLE III: Einstein radius crossing times for Bulge and LMC lensings. t_E is the Einstein radius crossing time. $D_S = 8kpc$ and $D_L = 4kpc$ are assumed for Bulge. $D_S = 50kpc$ and $D_L = 25kpc$ are assumed for LMC. $v_T = 220km/s$ is assumed for Bulge and LMC. In this table, the Einstein radius is calculated by $R_E = v_T \times t_E$ from the definition of the Einstein radius crossing time. Here, the input is $t_E \sim 10^{-3} - 10^3(day)$, namely $1(min.) - 3(yr.)$.

$t_E(day)$	$R_E(km)$	$\frac{\bar{\varepsilon}}{R_E^n}$ [Bulge]	$\frac{\bar{\varepsilon}}{R_E^n}$ [LMC]
10^{-3}	1.9×10^4	3.1×10^{-13}	5.0×10^{-14}
10^{-2}	1.9×10^5	3.1×10^{-12}	5.0×10^{-13}
10^{-1}	1.9×10^6	3.1×10^{-11}	5.0×10^{-12}
1	1.9×10^7	3.1×10^{-10}	5.0×10^{-11}
10	1.9×10^8	3.1×10^{-9}	5.0×10^{-10}
10^2	1.9×10^9	3.1×10^{-8}	5.0×10^{-9}
10^3	1.9×10^{10}	3.1×10^{-7}	5.0×10^{-8}